Modifications of Breakthrough Models for Fixed-bed Column and Insights into Physical Meanings of Corresponding Parameters

Modifications of Breakthrough Models for Fixed-bed Column and Insights into Physical Meanings of Corresponding Parameters

July 2019

Hu Qili

Modifications of Breakthrough Models for Fixed-bed Column and Insights into Physical Meanings of Corresponding Parameters

A Dissertation Submitted to

the Graduate School of Life and Environmental Sciences,

the University of Tsukuba

in Partial Fulfillment of the Requirements

for the Degree of Doctor of Philosophy in Environmental Studies

(Doctoral Program in Sustainable Environmental Studies)

Hu Qili

Abstract

Adsorption process is one of the most widely applied technologies for water reuse and wastewater treatment. It plays an important role in determining the distribution, migration, transformation and fate of water pollutants. Adsorption has been an indispensable unit operation in industrial application such as separation and purification, industrial catalysis and pollution control. Adsorption has long been favored by many researchers because of its low cost, fast kinetics, low energy for regeneration, insensitivity to toxic substances and complete removal of pollutants even from dilute solution. In the practical operation of full-scale adsorption process, a fixed-bed adsorption system is preferred. In such a system, adsorption of the solutes is a time- and distance-dependent process. The curvature and symmetry of the breakthrough curve are usually subjected to different adsorbent-adsorbate systems and operating conditions. How to accurately describe the breakthrough curve is still a problem that needs to be addressed urgently.

The design and optimization of an adsorption process often require the development of a mathematical model that can predict the breakthrough curve. This study tries to address the following problems: (i) Revelation of mathematical characteristics of the breakthrough curves by adjusting model parameters; (ii) Description of the heterogeneous diffusion-limited process based on the fractal-like kinetics and (iii) Establishment of empirical breakthrough models using hyperbolic tangent and double exponential functions.

In Chapter 2, maximum specific breakthrough rate μ_{max}, lag time λ, inflection point t_i and half-operating time t_{50} can reflect the curvature and symmetry of the breakthrough curves: Bohart–Adams, Thomas and Yoon–Nelson models represent the same symmetric breakthrough curve; Clark and dose-response models show an asymmetric breakthrough curve; and Wolborska model is not a sigmoidal curve. The physical meaning of q_0m/vc_0 and a_0x/uc_0 is the operating time required to reach 50% breakthrough. The graphic description of the breakthrough curves and rate profiles contributes to selecting the optimal model.

In Chapter 3, the fractal-like kinetics or time-dependent rate coefficient is introduced into Bohart–Adams, Thomas and Yoon–Nelson models to describe the heterogeneous diffusion-limited process in a fixed-bed column. The fitting performance of fractal-like breakthrough

models is validated by nitrate adsorption on chitosan-Fe(III) composite. Compared with the Bohart–Adams and Yoon–Nelson models (Adj. $R^2 = 0.9878$ and $\chi^2 = 1.37 \times 10^{-3}$), the fractal-like Bohart–Adams (Adj. $R^2 = 0.9989$ and $\chi^2 = 1.25 \times 10^{-4}$) and fractal-like Yoon–Nelson (Adj. $R^2 = 0.9992$ and $\chi^2 = 8.86 \times 10^{-5}$) models can better describe nitrate adsorption on chitosan-Fe(III) composite. The fractal-like breakthrough models can describe asymmetric breakthrough curves due to introduction of the fractal-like exponent h, which extends application scope of Bohart–Adams, Thomas and Yoon–Nelson models.

In Chapter 4, the hyperbolic tangent and double exponential models are proposed to simulate the dynamic behaviors in a fixed-bed column for the adsorption of a wide range of water pollutants. The parameters n, μ_{max} and λ are introduced to hyperbolic tangent and double exponential models to better express the curvature and symmetry of the breakthrough curve. The hyperbolic tangent and double exponential models represent symmetric and asymmetric breakthrough curves, respectively. The fitting performance of empirical breakthrough models is evaluated by nitrate adsorption on chitosan-Fe(III) composite. It is found that the double exponential model has best fitting performance with the largest adjusted determination factor (Adj. $R^2 = 0.9977$) and smallest reduced chi-squared value ($\chi^2 = 2.54 \times 10^{-4}$). The maximum specific breakthrough rate μ_{max}, lag time λ, inflection point t_i and half-operating time t_{50} predicted by the double exponential model are 3.99×10^{-3} min^{-1}, 29.7 min, 121.9 min and 155.7 min, respectively.

The practical significance of this study is to provide alternative methods for the modeling of continuous-flow fixed-bed adsorption. The description of mathematical characteristics of the breakthrough curves and rate profiles is beneficial to reveal the dynamic behaviors in a fixed-bed column. The revelation of mathematical relationships between breakthrough models greatly reduces the workload. The fractal-like Bohart–Adams, fractal-like Thomas and fractal-like Yoon–Nelson models can describe heterogeneous diffusions-limited processes. The hyperbolic tangent and double exponential models are important supplements of the adsorption kinetics. This study may help readers to better understand the adsorption process in a fixed-bed column and provide useful information for the design of adsorption systems.

***Keywords*:** Adsorption; Model parameters; Modification; Fixed bed; Breakthrough curve

Contents

List of Tables

List of Figures

Nomenclature

A	dimensionless Clark constant
a	dimensionless dose-response constant
a_0	adsorption capacity (mg L^{-1})
Adj. R^2	adjusted determination factor
b	dose-response constant ($b = vc_0/q_0m$)
c	effluent solute concentration (mg L^{-1})
c_0	influent solute concentration (mg L^{-1})
c_b	concentration of the solute at the breakthrough time (mg L^{-1})
f	number of degrees of freedom
h	fractal-like exponent, reflecting whether a system is homogeneous
k_0	fractal-like rate constant
k_{BA}	Bohart–Adams rate constant (mL min^{-1} mg^{-1})
$k_{BA,0}$	fractal-like Bohart–Adams rate constant (L mg^{-1} $min^{-(1-h)}$)
k_T	Thomas rate constant (mL min^{-1} mg^{-1})
K_T	mass-transfer coefficient (min^{-1})
$k_{T,0}$	fractal-like Thomas rate constant (L mg^{-1} $min^{-(1-h)}$)
k_{YN}	Yoon–Nelson rate constant (min^{-1})
$k_{YN,0}$	fractal-like Yoon–Nelson rate constant ($min^{-(1-h)}$)
m	absorbent mass filled in the column (g)
MTZ	mass transfer zone
n	Freundlich constant
n	number of data points
p	number of model parameters
q_0	saturation capacity (mg g^{-1})
r	Clark constant (min^{-1})
R^2	multiple coefficient of determination ($R^2 = 1 - RSS/TSS$)
RSS	residual sum of squares

t	operating time (min)
t_{50}	half-operating time (min)
t_b	breakthrough time (min)
t_i	inflection point (min)
t_s	saturation time (min)
TSS	total sum of squares
u	linear flow velocity (cm min^{-1})
U_0	flow rate per unit cross-sectional area of the column (mL min^{-1} cm^{-2})
v	flow rate (mL min^{-1})
x	bed height (cm)
y	c/c_0
y_{cal}	predicted value
y_{exp}	observed value
β_a	effective kinetic coefficient reflecting the effect of both axial dispersion and mass transfer (min^{-1})
λ	lag time (min)
μ_{max}	maximum specific breakthrough rate (min^{-1})
v_m	migration velocity of the concentration front in a fixed-bed column (cm min^{-1})
τ	operating time required to reach 50% breakthrough (min)
χ^2	reduced chi-square value
ω_i	weighting coefficient ($\omega_i = 1/y_i$)

Chapter 1 Introduction

1.1. Adsorption principles

In wastewater treatment, adsorption is a surface phenomenon that is generally defined as an enrichment of chemical species from aqueous solution on the solid surface (Worch, 2012). The adsorbate is attracted to the adsorbent surface due to the unbalanced forces, and thus the degrees of freedom and the surface free energy are reduced (Bonilla-Petriciolet et al., 2017). Adsorption plays an important role in determining the distribution, migration, transformation and fate of water pollutants such as heavy metals, inorganic nutrients and toxic organic matters. Adsorption method is one of the most widely used technologies for water reuse and wastewater treatment. It has long been favored by many researchers because of its low initial cost, simple design, facile operation, insensitivity to toxic substances and complete removal of contaminants even from dilute solution (Foo and Hameed, 2010). Adsorption has been an indispensable unit operation in industrial application including separation and purification, industrial catalysis and pollution control (Rouquerol et al., 2013).

1.1.1. Mass transfer

During the adsorption process, the mass transfer of the adsorbates from aqueous solution to the solid surface continues until the adsorption equilibrium to be reached between the two phases. The affinity of the adsorbent for different adsorbates determines the distribution of solutes in solid/solution phases. As shown in Figure 1-1, there are four steps associated with the uptake of adsorbates by porous adsorbents such as bulk transport, film diffusion, intraparticle diffusion and adsorptive attachment (Tran et al., 2017; Weber Jr, 1984). If one step contributes dominantly to the total resistance and the other steps marginally increases the adsorption rate, this step is called a rate-controlling step (Tan and Hameed, 2017).

In most cases, the bulk transport can occur rapidly after addition of the adsorbent and the first step is easily manipulated by mixing. Therefore, it does not control engineering design and its contribution to the mass transfer resistance is considered negligible. The adsorptive attachment usually occurs very quickly and thus is also not significant for design. The remaining two steps, either singly or in combination, are most commonly the rate-controlling

step (Weber and Smith, 1987). The film diffusion is the transport of the adsorbates to the exterior surface of the adsorbent through a boundary layer. The third step is the diffusion of the adsorbates within the pores of the adsorbent or along pore-wall surfaces, or both. A good understanding of the transport processes is essential to set rigorous and optimum criteria for adsorber design and operation, and to identify and control important system variables.

1.1.2. Types of adsorption

In the actual wastewater treatment, there are two main driving forces during the solute adsorption, i.e. the hydrophobicity of solute and the affinity of the adsorbent for solutes (Çeçen and Aktas, 2011). The most important factor for the adsorption intensity is the solubility of a dissolved substance. A hydrophilic substance tends to the water system and shows a poor adsorption ability. In contrast, a hydrophobic substance tends to be adsorbed rather than staying in water. In particular, the hydrophobic part of the molecule is adsorbed, while its hydrophilic part tends to stay in water for complex organic contaminants with hydrophobic and hydrophilic groups. The affinity of adsorption is primarily caused by van der Waals attraction or chemical interaction with the adsorbent. In general, the adsorption can be divided into physical and chemical adsorption according to the type of interaction that occurs between the adsorbent and adsorbate (Bonilla-Petriciolet et al., 2017; Çeçen and Aktas, 2011; Rouquerol et al., 2013).

The adsorption induced by van der Waals forces rather than sharing or exchange of electrons is called physical adsorption, which is independent of the electronic properties of the adsorbate and adsorbent molecules. In physical adsorption, multiple layers may be formed which have similar heats of adsorption. Compared with chemical adsorption, the adsorbate is less strongly attached to a specific site in physical adsorption and thereby physically adsorbed molecule can be free to move within the interface.

In chemical adsorption, the adsorbate undergoes chemical interaction with the adsorbent. It involves the form of a chemical bond, i.e. an exchange of electrons between specific surface sites and solute molecules. Chemically adsorbed adsorbates are not free to move on the surface or within the interface. Chemical adsorption is characterized by a high adsorption energy since the adsorbate forms strong localized bonds at active centers on the adsorbent. Only a single molecular layer can be chemically adsorbed. Lower energies are usually associated with

physical adsorption, while higher energies are related to chemical adsorption. However, it is very difficult to distinguish between physical and chemical adsorption. The comparison of physical and chemical adsorption is listed in Table 1-1.

1.2. Fixed-bed adsorption

The fixed-bed adsorption is a basic form of the dynamic operation. The fixed-bed adsorber is widely applied to the engineered adsorption processes because it can provide reliable information concerning the breakthrough time, loss of adsorption capacity during subsequent cycles, and acceptable flow rate (Yanyan et al., 2018). The solute adsorption is a time- and distance-dependent process in a fixed-bed column. During the adsorption process, each adsorbent particle can continuously hold the chemical species from the mobile phase before reaching the equilibrium state (Worch, 2012). This adsorption process proceeds successively, layer by layer, from the column inlet to the column outlet. However, due to the slow adsorption kinetics, there is no distinct boundary between loaded and unloaded adsorbent layers. The change in the concentration of target contaminant in the effluent over time is termed as the breakthrough curve (Chu, 2004). The shape of the breakthrough curve suffers from various factors such as mass transfer resistance, flow rate, equilibrium time and adsorption mechanisms. The most effective adsorption performance can be obtained when the shape of the breakthrough curve is as sharp as possible (Alberti et al., 2012). The study of the breakthrough curve can evaluate the performance of adsorbent particles, determine the mass transfer coefficient and understand the operating conditions of the fixed bed.

As shown in Figure 1-2, in a single-solute adsorption case, a fixed-bed column can be divided into three zones (Worch, 2012):

(i) Saturation zone

The first zone is located between the adsorber inlet and the mass transfer zone (MTZ), and the adsorbent is already loaded with the adsorbate to the adsorbed amount q_0, which is in equilibrium with the inlet concentration c_0. In this zone, the available adsorption capacity is exhausted, and no more mass transfer from the liquid phase to the adsorbent particles takes place. Thus, the adsorption of contaminants reaches dynamic equilibrium at the solid/solution

interface;

(ii) Mass transfer zone

In the MTZ, the mass transfer from the liquid phase to the solid phase just occurs. Along the column, the concentration decreases from $c = c_0$ to $c = 0$, and the adsorbed amount increases from $q = 0$ to $q = q_0$. Shape and length of the MTZ are dependent of the adsorption rate and the shape of the equilibrium curve.

(iii) Adsorption zone

The adsorbent in this zone does not hold the adsorbates, and the fluid-phase concentration is $c = 0$.

As shown in Figure 1-2, the MTZ moves toward along the adsorber with a velocity that is much slower than the water velocity. The strong affinity of the adsorbent for the adsorbate results in the great difference between the MTZ velocity and the water velocity. As long as the MTZ has not reached the adsorber outlet, the outlet concentration is $c = 0$. The adsorbate begins to occurs in the adsorber outlet when the MTZ reaches the end of the adsorber. The required time is referred to as the breakthrough time t_b. As the adsorption progresses, the effluent concentration increases and the residual adsorbent capacity decreases. If the entire MTZ has left the adsorber, the effluent concentration equals c_0, in which all adsorbent particles are saturated and no net adsorption takes place. This time is referred to as saturation time t_s. Due to the asymptotic form of the breakthrough curve, the breakthrough time and the saturation time can not be determined exactly by the breakthrough models. Hence, the operating times at $c/c_0 = 0.05$ and $c/c_0 = 0.95$ are usually defined as the breakthrough time t_b and the saturation time t_s, respectively (de Franco et al., 2017).

In general, the degree of curvature and symmetry of the breakthrough curve are subjected to different adsorbent-adsorbate systems and operating conditions such as initial concentration, flow rate, bed height, particle size and pH (Ataei-Germi and Nematollahzadeh, 2016; Jang and Lee, 2016; Yanyan et al., 2018). A good understanding of the breakthrough behavior of the adsorbates to be removed is the essential precondition for any fixed-bed adsorber design. Therefore, how to accurately describe the breakthrough curve is still a problem to be addressed urgently.

1.3. Breakthrough models

The appropriate design of an adsorption process requires the development of a mathematical model that can describe the dynamic adsorption behaviors and predict the breakthrough curve in a fixed-bed column (Shafeeyan et al., 2014). One approach has been to solve simultaneously the partial differential equations (PDEs) describing the mass and the heat balance (Sircar and Kumar, 1983). However, the simultaneous solution of PDEs for a given adsorption system, although more general and mathematically rigid, requires complicated numerical solutions. Thus, in order to simulate the breakthrough behavior of a fixed-bed column with a high degree of accuracy, the use of simpler and more tractable models that avoid the need for numerical solution appears more suitable and logical in practice (Chu, 2004). Many attempts have been made to develop simplified breakthrough models to reduce computational time and facilitate optimization studies. These simplified breakthrough models are primarily established on the basis of the description of mass transfer within adsorption systems and they can describe the experimental data satisfactorily for most practical design purposes.

1.3.1. Bohart–Adams model

The Bohart–Adams model is initially used to describe the adsorption of chlorine on charcoal in a continuous-flow system and assumes that the rate of reaction is proportional to the residual adsorption capacity of the adsorbent and to the concentration of the adsorbate in the mobile phase (Bohart and Adams, 1920). The integral form of the Bohart–Adams model is expressed as:

$$\frac{c}{c_0} = \frac{\exp(k_{\mathrm{BA}} c_0 t)}{\exp\left(\frac{k_{\mathrm{BA}} a_0 x}{u}\right) + \exp(k_{\mathrm{BA}} c_0 t) - 1} \tag{1-1}$$

Compared with the first two exponential terms in the denominator, if the last term is negligible, Eq. (1-1) reduces to

$$\frac{c}{c_0} = \frac{1}{1 + \exp\left(\frac{k_{\mathrm{BA}} a_0 x}{u} - k_{\mathrm{BA}} c_0 t\right)} \tag{1-2}$$

1.3.2. Thomas model

The Thomas model is widely used to predict breakthrough curves at various bed depths, flow rates, and initial solute concentrations in a fixed-bed column (Yan et al., 2017). It assumes

that: (i) Plug flow behavior occurs during the adsorption process (Gong et al., 2015); (ii) Adsorption is limited by mass transfer with no axial dispersion at the solid/solution interface (Nandanwar et al., 2017); and (iii) The experimental data follows the Langmuir isotherm and second-order reversible reaction kinetics (Ataei-Germi and Nematollahzadeh, 2016). The Thomas model is appropriate to evaluate the adsorption process where external and internal diffusion resistances are extremely small, which can be written as:

$$\frac{c}{c_0} = \frac{1}{1 + \exp\left(\frac{k_T q_0 m}{v} - k_T c_0 t\right)} \tag{1-3}$$

1.3.3. Yoon–Nelson model

The Yoon–Nelson model assumes that the rate of decrease in the probability of adsorption for each adsorbate is proportional to the probability of adsorption and the probability of breakthrough (Yoon and Nelson, 1984). It is a relatively simple model and does not require detailed data with respect to the characteristics of the adsorbates, the type of adsorbent and the physical properties of the adsorption bed (Soto et al., 2017). The Yoon–Nelson model can be expressed as:

$$\frac{c}{c_0} = \frac{1}{1 + \exp[k_{YN}(\tau - t)]} \tag{1-4}$$

1.3.4. Clark model

In 1987, Clark develops a model to evaluate adsorption performance of granular activated carbon (GAC) for the removal of organic compounds in a fixed-bed column (Clark, 1987). It assumes that: (i) The adsorption process obeys the Freundlich isotherm; (ii) An ideal mass balance over the entire column is based on all the solutes are removed in the outlet; (iii) Liquid phase mass balance equation is established using the mass-transfer concept.

$$\frac{c}{c_0} = \frac{1}{[1 + A\exp(-rt)]^{\frac{1}{n-1}}} \tag{1-5}$$

1.3.5. Dose-response model

It has been proved that a comparatively larger deviation exists between the experimental data and the predicted values when the Thomas model is used to analyze the experimental data (Yan et al., 2001). Therefore, the dose-response model is proposed to minimize the error resulting from the Thomas model, which can be expressed as:

$$\frac{c}{c_0} = 1 - \frac{1}{1 + (bt)^a} \tag{1-6}$$

1.3.6. Wolborska model

The Wolborska model is based on the application of equations of mass transfer for diffusion mechanisms used for the low concentration breakthrough curve (Sana and Jalila, 2017), It is originally used to describe *p*-nitrophenol adsorption on activated carbon in a fixed-bed column, which can be given as (Wolborska, 1989):

$$\frac{c}{c_0} = \exp\left(\frac{\beta_a c_0}{a_0} t - \frac{\beta_a}{u} x\right) \tag{1-7}$$

1.4. Research problems

In the last two decades, great progress has been made in the field of adsorption. Most researchers mainly focus on the development of novel adsorption materials, evaluation of adsorption performance, synergistic or competitive effects of multicomponent adsorption, revelation of adsorption mechanisms and regeneration of contaminants-loaded adsorbent. However, few attentions are paid to the development of continuous-flow breakthrough models. The Bohart–Adams, Thomas, Yoon–Nelson, Clark, dose-response and Wolborska models are widely employed to simulate a fixed-bed adsorption system in wastewater treatment due to simple mathematical expressions and good fitting performance. The previous work aims to compare fitting performance between breakthrough models and estimate the model parameters, but there are still many problems to be addressed, including (i) Mathematical characteristics of the breakthrough curves such as the curvature and symmetry; (ii) Mathematical relationships between breakthrough models; (iii) Effects of model parameters on breakthrough curve and rate profile; (iv) Establishment of fractal-like and empirical breakthrough models; and (v) Physical meanings of model parameters.

1.5. Research objectives and thesis structure

This study aims to provide alternative methods to analyze a continuous-flow adsorption system through modifications of traditional breakthrough models and adaptation of some sigmoidal functions. The main objectives are:

(1) To intuitively reveal mathematical characteristics of breakthrough curve, including the degree of curvature and symmetry;

(2) To reveal mathematical relationships between breakthrough models and thus reduce the calculation amount significantly;

(3) To discuss effects of model parameters on breakthrough curves and rate profiles and thereby reveal physical meanings of some parameters or terms;

(4) To establish fractal-like breakthrough models to describe heterogeneous diffusion-limited adsorption processes and also propose some empirical breakthrough models to adapt to different adsorbent-adsorbate systems in a fixed-bed column based on hyperbolic tangent and double exponential functions;

(5) To highlight mistakes and controversies with respect to application of Bohart–Adams and Wolborska models to avoid this situation where they are repeated in subsequent publications.

In the first part of this study (Chapter 2), the main research contents include: (i) Mathematical relationships between traditional breakthrough models; (ii) Modifications of breakthrough models using the parameters μ_{max} and λ; (iii) Effects of model parameters on breakthrough curves and rate profiles and (iv) Physical meanings of model parameters. In the second part (Chapter 3), this study establishes fractal-like breakthrough models through the introduction of the fractal-like concept into Bohart–Adams, Thomas and Yoon–Nelson models; The fitting performance of fractal-like breakthrough models is evaluated by the adsorption of nitrate on chitosan-Fe(III) composite; and the degree of curvature and symmetry of breakthrough curves are investigated by adjusting the fractal-like exponent h. In the third part (Chapter 4), this study establishes empirical breakthrough models based on hyperbolic tangent and double exponential functions and evaluate their fitting performance. The whole structure of this thesis is described in Figure 1-3.

Table 1-1 Comparison of physical and chemical adsorption.

Category	Physical adsorption	Chemical adsorption
Electron transfer or sharing	No	Yes
Interaction	van der Waals, hydrogen bonds	Ionic or covalent bonds
Coverage	Mono- or multi-layer	Mono-layer
Nature of adsorption	Nondissociative and reversible	Often dissociative and irreversible
Degree of Specificity	Low	Very high
Temperature-dependent uptake	Decreases	Increases
Adsorption enthalpy	5–40 kJ mol^{-1}	40–800 kJ mol^{-1}
Adsorption kinetics	Fast	Very variable, often slow
Desorption	Easy	Difficult
Desorbed species	Adsorbate unchanged	Adsorbate may change

Data from Bonilla-Petriciolet et al., 2017; Çeçen and Aktas, 2011; Rouquerol et al., 2013.

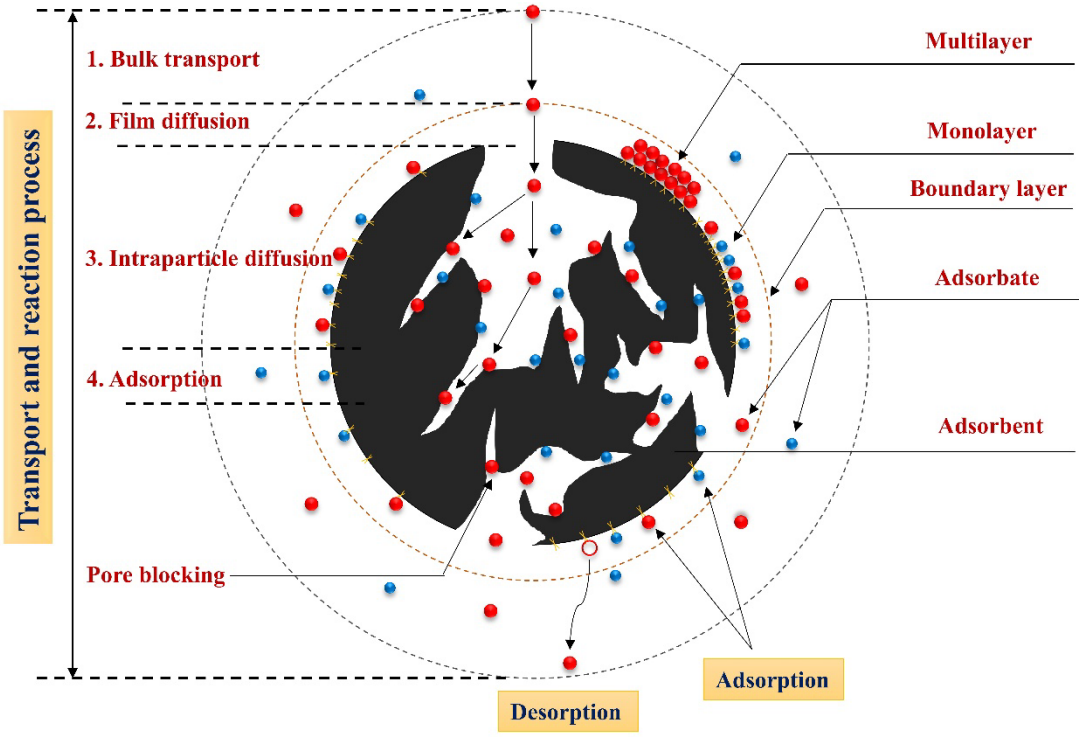

Figure 1-1 Schematic diagram of transport and reaction processes by porous adsorbents (Adapted from Tran et al., 2017; Weber Jr, 1984).

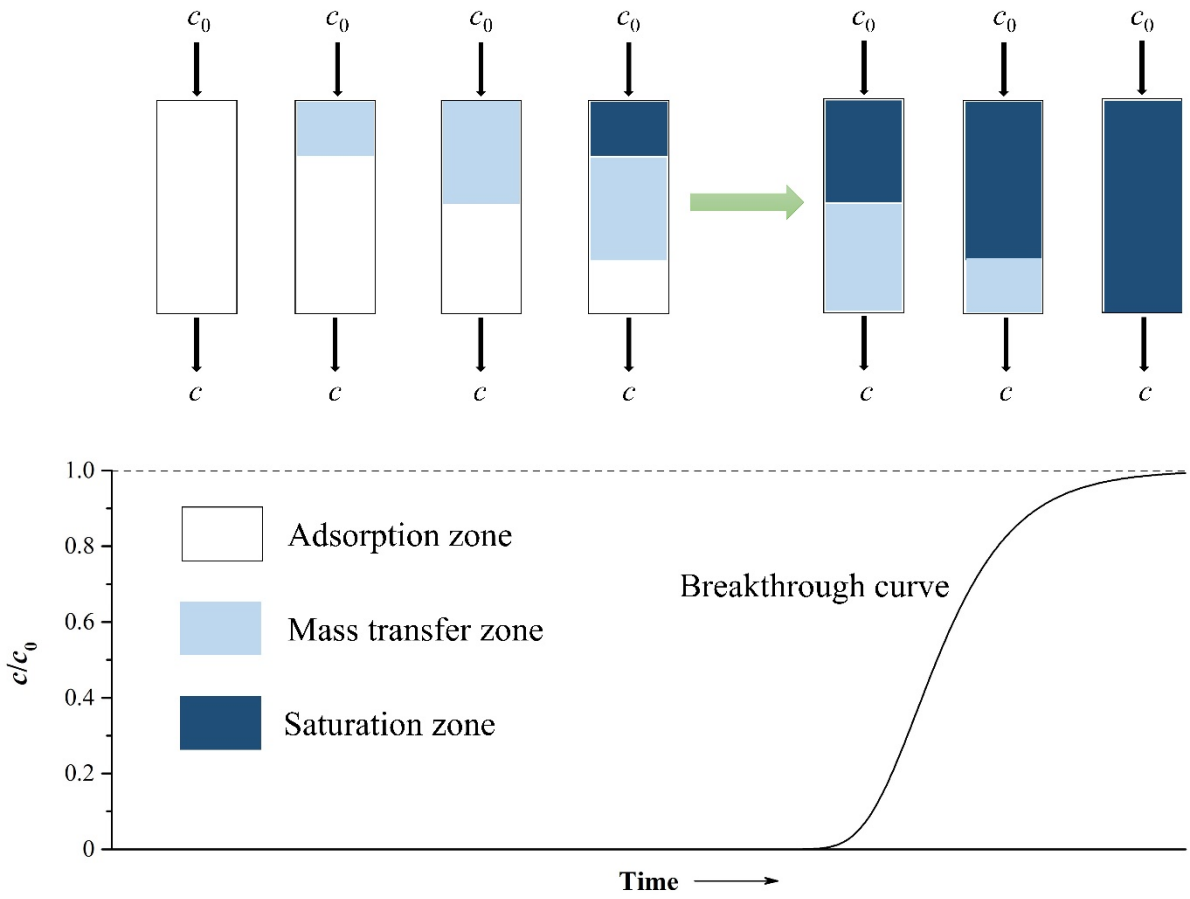

Figure 1-2 Traveling of mass transfer zone through a fixed-bed column and development of a breakthrough curve (Adapted from Worch, 2012).

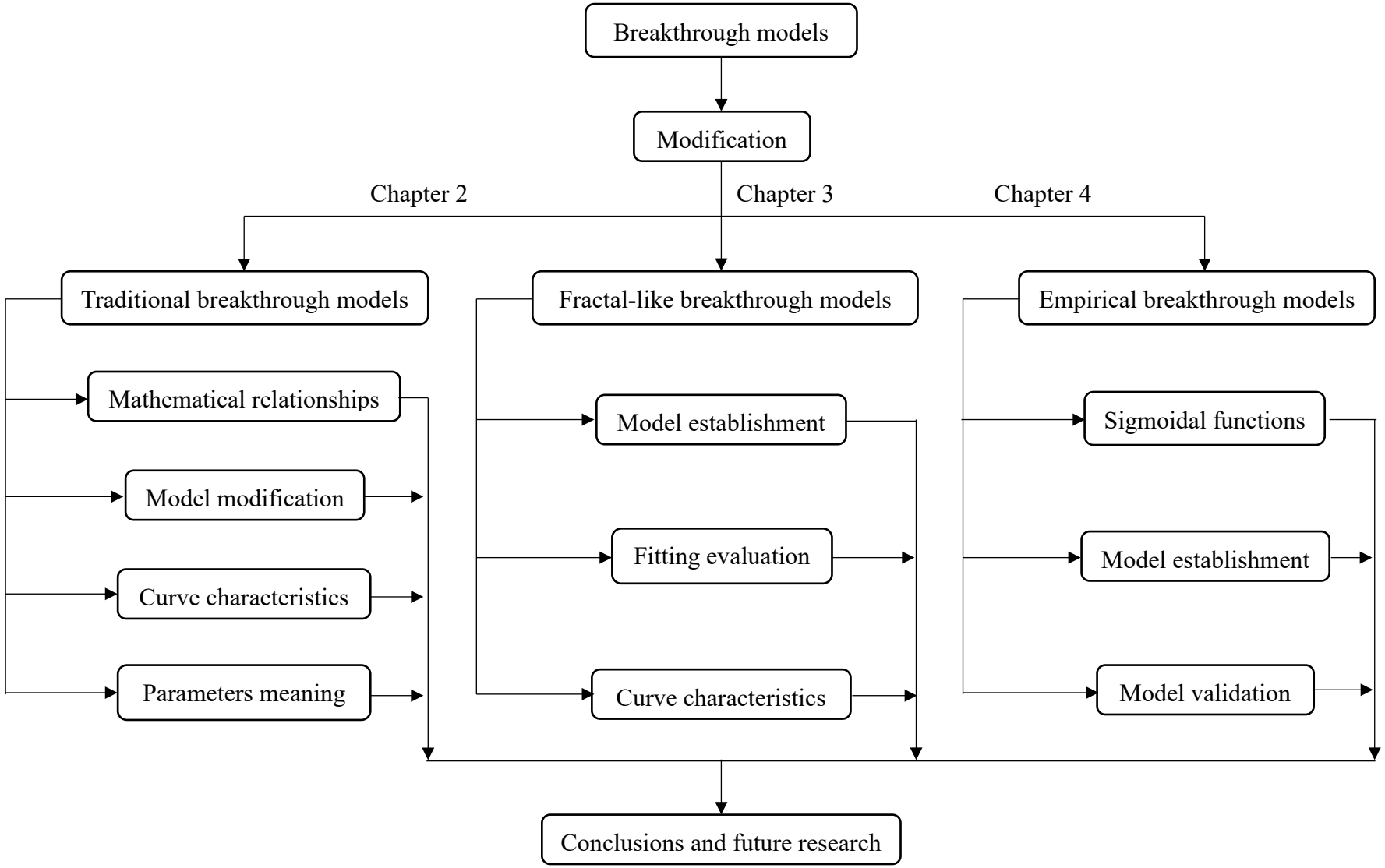

Figure 1-3 Research route and framework of this thesis.

Chapter 2 Modification of breakthrough models and physical meanings of corresponding parameters in a fixed-bed column

2.1. Introduction

The Bohart–Adams, Thomas, Yoon–Nelson, Clark, dose-response and Wolborska models receive widespread concern by many researchers due to simple mathematical forms and good fitting performance. Ever since these breakthrough models were developed, they have been successfully applied to water and wastewater treatment in a wide range of pollutants, including heavy metals (Shahbazi et al., 2011), inorganic anions (Sun et al., 2014) and dyes (Ataei-Germi and Nematollahzadeh, 2016). However, many researchers only focus on the fitting performance of these breakthrough models and the determination of the model parameters. The mathematical laws followed by the models themselves is usually ignored.

Some crucial problems are to be addressed when the breakthrough models are fitted to the experimental data: (i) mathematical relationships between breakthrough models; (ii) physical meanings of model parameters; (iii) effects of model parameters on the breakthrough curve and rate profile; (iv) complete description of the breakthrough curve; and (v) establishment of new breakthrough models. In addition, a controversy concerning application of the Bohart–Adams and Wolborska models occurs in scientific literature. Once the controversy enters the literature, it is very difficult to eradicate it and is unavoidably repeated in subsequent publications. In order to avoid this situation, it is extremely necessary to highlight this controversy.

2.2. Mathematical relationships between breakthrough models

In many published research papers (Darweesh and Ahmed, 2017; Gong et al., 2015; Jang and Lee, 2016; Nguyen et al., 2015), it is found that the breakthrough curves are not coincident and the error values are not identical when the Bohart–Adams, Thomas and Yoon–Nelson models are used to correlate with the experimental data in a fixed-bed adsorption system, implying that the three breakthrough models are separate and independent. But, it is not the case. In order to facilely observe mathematical characteristics of the Bohart–Adams, Thomas and Yoon–Nelson models, the three breakthrough models are rewritten as:

$$\frac{c}{c_0} = \frac{1}{1 + \exp\left[k_{\mathrm{BA}} c_0 \left(\frac{a_0 x}{u c_0} - t\right)\right]} \tag{2-1}$$

$$\frac{c}{c_0} = \frac{1}{1 + \exp\left[k_{\mathrm{T}} c_0 \left(\frac{q_0 m}{v c_0} - t\right)\right]} \tag{2-2}$$

$$\frac{c}{c_0} = \frac{1}{1 + \exp[k_{\mathrm{YN}}(\tau - t)]} \tag{2-3}$$

One can readily see that the terms $k_{\mathrm{BA}}c_0$, $k_{\mathrm{T}}c_0$ and k_{YN} have the identical dimension of reciprocal time (min^{-1}), while the terms a_0x/uc_0, q_0m/vc_0 and τ also have the same dimension of time (min). As a consequence, the following relationships are acceptable.

$$k_{\mathrm{YN}} = k_{\mathrm{T}} c_0 = k_{\mathrm{BA}} c_0 \tag{2-4}$$

$$\tau = \frac{q_0 m}{v c_0} = \frac{a_0 x}{u c_0} \tag{2-5}$$

It follows that the Bohart–Adams, Thomas and Yoon–Nelson models are equivalent and represent a logistic function in mathematical nature. Thus, the breakthrough curves represented by the three breakthrough models are coincident and all error values are equal when the curve fitting is carried out. The significance of the revelation of this relationships consists in: (1) the physical meanings of the terms q_0m/vc_0 and a_0x/uc_0 are the operating time required to reach 50% breakthrough and k_{YN} is numerically equal to a product of k_{BA} (k_{T}) and c_0; (2) k_{YN} and τ directly used to calculate k_{BA} (k_{T}) and a_0 (q_0) can significantly reduce workload instead of the complex curve fitting. The Yoon–Nelson model does not require detailed data with respect to the characteristics of adsorbates, the type of an adsorbent and the physical properties of a fixed-bed column, indicating that the parameters k_{YN} and τ may be regarded as lumped parameters that embed some operating features.

There are two controversies with respect to the Bohart–Adams model that need to be specifically pointed out. It is debatable to regard Eq. (2-1) as the bed depth service time (BDST) model initially proposed by Hutchins (Hutchins, 1973) in some published research papers (Kundu and Gupta, 2005; Uddin et al., 2009; Unuabonah et al., 2010; Yang et al., 2015). After reading the original paper carefully (Bohart and Adams, 1920), it is found that Eq. (2-1) actually belongs to the work of Bohart and Adams. On the other hand, some research papers give another form of the Bohart–Adams model (Jang and Lee, 2016; Wang et al., 2015; Yan et al., 2017):

$$\frac{c}{c_0} = \exp\left[k_{\mathrm{BA}} c_0 \left(t - \frac{a_0 x}{u c_0}\right)\right] \tag{2-6}$$

It is not difficult to find that Eq. (2-6) is a further simplified form of Eq. (2-1) when the first term in the denominator is negligible compared with the exponential term. However, this simplified method changes the mathematical laws followed by Eq. (2-1). As shown in Figure 2-1, Eq. (2-1) and Eq. (2-6) are derived from a standard logistic function $y = 1/(1+\exp(-t))$ and an exponential function $y = \exp(t)$ respectively by the stretching and translation transformations in sequence. It is obvious that the breakthrough curve given by Eq. (2-6) is not an asymptotic S-shaped curve. Generally speaking, in order to obtain good fitting performance, distribution of the experimental data must approach the shape of the curve represented by the breakthrough model (Harter, 1984). Therefore, Eq. (2-6) is not appropriate for the description of the breakthrough curve within the whole adsorption time and thus k_{BA} and a_0 obtained from Eq. (2-6) do not reflect an actual fixed-bed adsorption system. By contrast, it is observed from Figure 2-1 that the breakthrough curve provided by Eq. (2-1) is an asymptotic S-shaped curve that it is centrosymmetric with respect to one point (a_0x/uc_0, 0.5) in rectangular coordinates. This type of the breakthrough curve can well reflect actual fixed-bed adsorption systems and describe the dynamic behaviors during the adsorption process.

It can be clearly seen from Eq. (1-5) that the Clark model can also reduce to a logistic function ($A = r = 1$ and $n = 2$). Thus, the Clark model can be transformed to the Bohart–Adams, Thomas or Yoon–Nelson model through the appropriate variable substitution when $n = 2$.

$$A = \exp\left(\frac{k_{\mathrm{BA}} a_0 x}{u}\right) = \exp\left(\frac{k_{\mathrm{T}} q_0 m}{v}\right) = \exp(k_{\mathrm{YN}}\tau) \tag{2-7}$$

$$r = k_{\mathrm{BA}} c_0 = k_{\mathrm{T}} c_0 = k_{\mathrm{YN}} \tag{2-8}$$

It follows that the Clark model can be seen as a generalized form of the Bohart–Adams, Thomas and Yoon–Nelson models. The Clark model may provide better fitting performance since an extra adjustable parameter n make the curve fitting more flexible.

It is worth noting that Eq. (1-7) and Eq. (2-6) have the same mathematical structure. Thus, the Wolborska model can be also derived from an exponential function $y = \exp(t)$ by stretching and translation transformations. That is, the Wolborska model does not represent a S-shaped

curve. The parameters β_a and a_0 does not reflect an actual fixed-bed adsorption system, either. Consequently, the use of Eq. (1-7) and Eq. (2-6) should be avoided because they fail to describe the breakthrough curve completely. The revelation of the mathematical relationships between the breakthrough models contributes to the appropriate selection of the models and precise calculation of model parameters.

2.3. Modification of breakthrough models

Similar to the bacterial growth curve (Zwietering et al., 1990), the breakthrough curve can be also divided into three phases (Figure 2-2): Lag, logarithmic and stationary phases. In the lag phase, the fresh adsorbents packed in a fixed-bed column contain large numbers of available adsorption sites and thereby hold the adsorbate molecules consecutively, leading to the very low effluent concentration; In the logarithmic phase, as the adsorption progresses, the decrease in adsorption sites results in the rapid increase in the effluent concentration; In the stationary phase, the adsorbent particles approach the saturation state gradually and thus the effluent concentration tends to a stationary value. The three phases of the breakthrough curve can be described by three parameters: Lag time λ, maximum specific breakthrough rate μ_{max} and influent concentration c_0. Herein, μ_{max} and λ are defined as the slope of the tangent line at the inflection point of the breakthrough curve and the t-axis intercept of this tangent line, respectively. μ_{max} can reflect whether the adsorption is favorable and λ represents the required operating time when the breakthrough curve begins to rise significantly.

It is difficult to accurately calculate them if the parameters μ_{max} and λ are not estimated directly in the equation. Therefore, in order to effectively estimate μ_{max} and λ, all breakthrough models are modified by substituting the model parameters with μ_{max} and λ. The detailed derivation processes are as follows.

2.3.1. Modified Yoon–Nelson model

In order to introduce μ_{max} and λ into the Yoon–Nelson model (Eq. (2-3)), let $y = c/c_0$, and then the first and second derivatives with respect to t are given as:

$$\frac{dy}{dt} = \frac{k_{YN} \cdot \exp[k_{YN}(\tau - t)]}{\{1 + \exp[k_{YN}(\tau - t)]\}^2} \tag{2-9}$$

$$\frac{\mathrm{d}^2 y}{\mathrm{d}t^2} = \frac{{k_{\mathrm{YN}}}^2 \cdot \exp[k_{\mathrm{YN}}(\tau - t)] \cdot \{\exp[k_{\mathrm{YN}}(\tau - t)] - 1\}}{\{1 + \exp[k_{\mathrm{YN}}(\tau - t)]\}^3} \tag{2-10}$$

The second derivative is equal to zero at the inflection point $t = t_i$.

$$\left.\frac{\mathrm{d}^2 y}{\mathrm{d}t^2}\right|_{t=t_i} = 0 \Longrightarrow t_i = \tau \tag{2-11}$$

The maximum specific breakthrough rate $\mu_{\max}$ can be obtained by calculating the first derivative at $t = t_i$.

$$\mu_{\max} = \left.\frac{\mathrm{d}y}{\mathrm{d}t}\right|_{t=t_i} = \frac{k_{\mathrm{YN}}}{4} \tag{2-12}$$

The description of the tangent line through the inflection point is:

$$y = \frac{k_{\mathrm{YN}}}{4}(t - \tau) + 0.5 \tag{2-13}$$

The lag time is given as:

$$\frac{k_{\mathrm{YN}}}{4}(\lambda - \tau) + 0.5 = 0 \Longrightarrow \lambda = \tau - \frac{2}{k_{\mathrm{YN}}} \tag{2-14}$$

The half-operating time is written as:

$$t_{50} = \tau \tag{2-15}$$

Eq. (2-12) and Eq. (2-14) are rewritten as:

$$k_{\mathrm{YN}} = 4\mu_{\max} \tag{2-16}$$

$$\tau = \lambda - \frac{1}{2\mu_{\max}} \tag{2-17}$$

Substitution of Eq. (2-16) and Eq. (2-17) into Eq. (2-3) leads to

$$\frac{c}{c_0} = \frac{1}{1 + \exp\left[4\mu_{\max}(\lambda - t) + 2\right]} \tag{2-18}$$

As mentioned above, the Bohart–Adams, Thomas and Yoon–Nelson models represent the same breakthrough curve according to Eq. (2-4) and Eq. (2-5). Thus, Eq. (2-18) also belongs to the modified Bohart–Adams and modified Thomas models.

2.3.2. Modified Clark model

According to the above procedure, let $y = c/c_0$, the first and second derivatives of the Clark model (Eq. (1-5)) with respect to t are given as:

$$\frac{\mathrm{d}y}{\mathrm{d}t} = \frac{Ar}{n-1} \cdot \exp(-rt) \cdot [1 + A\exp(-rt)]^{-\frac{n}{n-1}} \tag{2-19}$$

$$\frac{\mathrm{d}^2y}{\mathrm{d}t^2} = \frac{Ar^2}{n-1} \cdot \exp(-rt) \cdot [1 + A\exp(-rt)]^{-\frac{2n-1}{n-1}} \cdot \left[\frac{A}{n-1} \cdot \exp(-rt) - 1\right] \tag{2-20}$$

The second derivative is equal to zero at the inflection point $t = t_i$.

$$\left.\frac{\mathrm{d}^2y}{\mathrm{d}t^2}\right|_{t=t_i} = 0 \Longrightarrow t_i = -\frac{1}{r}\ln\left(\frac{n-1}{A}\right) \tag{2-21}$$

Substitution of Eq. (2-21) into Eq. (2-19) leads to

$$\mu_{\max} = \left.\frac{\mathrm{d}y}{\mathrm{d}t}\right|_{t=t_i} = r \cdot n^{-\frac{n}{n-1}} \tag{2-22}$$

The description of the tangent line through the inflection point is:

$$y = r \cdot n^{-\frac{n}{n-1}}\left[t + \frac{1}{r}\ln\left(\frac{n-1}{A}\right)\right] + n^{-\frac{1}{n-1}} \tag{2-23}$$

The lag time is given as:

$$r \cdot n^{-\frac{n}{n-1}}\left[\lambda + \frac{1}{r}\ln\left(\frac{n-1}{A}\right)\right] + n^{-\frac{1}{n-1}} = 0 \Longrightarrow \lambda = -\frac{1}{r}\left[\ln\left(\frac{n-1}{A}\right) + n\right] \tag{2-24}$$

The half-operating time is written as:

$$t_{50} = -\frac{1}{r}\ln\left(\frac{2^{n-1}-1}{A}\right) \tag{2-25}$$

Eq. (2-22) and Eq. (2-24) are rewritten as:

$$r = \mu_{\max} \cdot n^{\frac{n}{n-1}} \tag{2-26}$$

$$A = (n-1) \cdot \exp\left[\lambda\mu_{\max} \cdot n^{\frac{n}{n-1}} + n\right] \tag{2-27}$$

Substitution of Eq. (2-26) and Eq. (2-27) into Eq. (1-5) leads to

$$\frac{c}{c_0} = \frac{1}{\left\{1 + (n-1) \cdot \exp\left[\mu_{\max} \cdot n^{\frac{n}{n-1}}(\lambda - t) + n\right]\right\}^{\frac{1}{n-1}}} \tag{2-28}$$

2.3.3. Modified dose-response model

According to the above procedure, let $y = c/c_0$, the first and second derivatives of the dose-response model (Eq. (1-6)) with respect to t are given as:

$$\frac{\mathrm{d}y}{\mathrm{d}t} = \frac{ab \cdot (bt)^{a-1}}{[1 + (bt)^a]^2} \tag{2-29}$$

$$\frac{\mathrm{d}^2 y}{\mathrm{d}t^2} = \frac{ab^2 \cdot (bt)^{a-2} \cdot [(a+1) \cdot (bt)^a - a + 1]}{[1 + (bt)^a]^3} \tag{2-30}$$

The second derivative is equal to zero at the inflection point $t = t_i$.

$$\left.\frac{\mathrm{d}^2 y}{\mathrm{d}t^2}\right|_{t=t_i} = 0 \Longrightarrow t_i = \frac{1}{b}\left(\frac{a-1}{a+1}\right)^{\frac{1}{a}} \tag{2-31}$$

The maximum specific breakthrough rate $\mu_{\max}$ can be obtained by calculating the first derivative at $t = t_i$.

$$\mu_{\max} = \left.\frac{\mathrm{d}y}{\mathrm{d}t}\right|_{t=t_i} = \frac{b}{4a} \cdot (a-1)^{\frac{a-1}{a}} \cdot (a+1)^{\frac{a+1}{a}} \tag{2-32}$$

The description of the tangent line through the inflection point is:

$$y = \frac{b}{4a} \cdot (a-1)^{\frac{a-1}{a}} \cdot (a+1)^{\frac{a+1}{a}} \left[t - \frac{1}{b}\left(\frac{a-1}{a+1}\right)^{\frac{1}{a}}\right] + \frac{a-1}{2a} \tag{2-33}$$

The lag time is given as:

$$\frac{b}{4a} \cdot (a-1)^{\frac{a-1}{a}} \cdot (a+1)^{\frac{a+1}{a}} \left[\lambda - \frac{1}{b}\left(\frac{a-1}{a+1}\right)^{\frac{1}{a}}\right] + \frac{a-1}{2a} = 0 \tag{2-34}$$

Eq. (2-34) is rewritten as:

$$\lambda = \frac{1}{b}\left(\frac{a-1}{a+1}\right)^{\frac{a+1}{a}} \tag{2-35}$$

The half-operating time is given as:

$$t_{50} = \frac{1}{b} \tag{2-36}$$

Eq. (2-32) and Eq. (2-35) are rewritten as:

$$a = \left(\lambda\mu_{\max} + \sqrt{1 + \lambda\mu_{\max}}\right)^2 \tag{2-37}$$

$$b = \frac{1}{\lambda}\left[\frac{\left(\lambda\mu_{\max} + \sqrt{1 + \lambda\mu_{\max}}\right)^2 - 1}{\left(\lambda\mu_{\max} + \sqrt{1 + \lambda\mu_{\max}}\right)^2 + 1}\right]^{1 + \frac{1}{\left(\lambda\mu_{\max} + \sqrt{1+\lambda\mu_{\max}}\right)^2}} \tag{2-38}$$

Substitution of Eq. (2-37) and Eq. (2-38) into Eq. (1-6) leads to

$$\frac{c}{c_0} = 1 - \frac{1}{1 + \left\{ \frac{t}{\lambda} \left[\frac{\left(\lambda\mu_{\max} + \sqrt{1+\lambda\mu_{\max}}\right)^2 - 1}{\left(\lambda\mu_{\max} + \sqrt{1+\lambda\mu_{\max}}\right)^2 + 1} \right]^{1+\frac{1}{\left(\lambda\mu_{\max} + \sqrt{1+\lambda\mu_{\max}}\right)^2}} \right\}^{\left(\lambda\mu_{\max} + \sqrt{1+\lambda\mu_{\max}}\right)^2}} \tag{2-39}$$

As mentioned above, the Wolborska model is not a S-shaped curve. As a result, it has no corresponding modified model. All breakthrough models in this study are showed in Table 2-1. It should be emphasized that modified breakthrough models are derived by variable substitution. Thus, the fitting curves are coincident and all error values are equal between the Bohart–Adams, Thomas, Yoon–Nelson, Clark, dose-response models and the corresponding modified breakthrough models.

2.4. Symmetry of breakthrough models

In this study, the inflection point t_i and half-operating time t_{50} are proposed to identify the symmetry of the breakthrough curve. Herein, t_i and t_{50} are defined as the operating time required to reach one point where the shape of the breakthrough curve is converted from the concave to the convex and 50% breakthrough (c/c_0 = 0.5), respectively. It is important to note that the above derivation processes also reveal the mathematical relationships between the defined four parameters and model parameters, which are listed in Table 2-2.

The relative magnitude of t_i and t_{50} can reflect the symmetry of the breakthrough curve. The Bohart–Adams, Thomas and Yoon–Nelson models can be derived from a logistic model. Thus, the three breakthrough models represent a symmetric breakthrough curve and t_i and t_{50} are equal.

For the Clark and dose-response models, the magnitude of $t_{50} - t_i$ can be given as:

$$t_{50} - t_i = \frac{1}{r} \ln\left(\frac{n-1}{2^{n-1}-1}\right) \tag{2-40}$$

$$t_{50} - t_i = \frac{1}{b}\left[1 - \left(\frac{a-1}{a+1}\right)^{\frac{1}{a}}\right] \tag{2-41}$$

It is obvious that the positive or negative value of $t_{50} - t_i$ only depends on the parameters n and a respectively. In the Clark model, the parameter n represents a Freundlich constant and the value of n lying in the range of 1–10 confirms the favorable condition for adsorption (Preethi

et al., 2017). A plot of $t_{50} - t_i$ as a function of n is described in Figure 2-3a. It is found that $1 < n < 2$, $t_{50} > t_i$; $n = 2$, $t_{50} = t_i$; and $2 < n < 10$, $t_{50} < t_i$. Thus, the Clark model can describe an asymmetric breakthrough curve when $n \neq 2$, and the breakthrough curve becomes more asymmetric when the parameter n deviates from 2.

In the dose-response model, the influence of the parameter a on the breakthrough curve is shown in Figure 2-4. All breakthrough curves for different a values passes through one point ($1/b$, 0.5) and the shape of the curves is dependent of the parameter a value. The dose-response model does not represent a S-shaped curve but exhibit a parabola-like curve when $a \leq 1$. The S-shaped curve occurs only at $a > 1$ and the degree of curvature becomes larger with the increase in a. It is observed from Figure 2-3b that $a > 1$, $t_{50} > t_i$. Therefore, the dose-response model provides an asymmetric breakthrough curve. The breakthrough curve approaches a symmetric curve since t_i is closer to t_{50} with the increase in a.

2.5. Breakthrough curve and rate profile

The breakthrough curve and rate profile of the Yoon–Nelson model for different k_{YN} are illustrated in Figure 2-5. All of the breakthrough curves pass through one point (τ, 0.5) and the degree of curvature increases with the increase in k_{YN} (become steeper). Each rate profile is a symmetric Gaussian distribution shape concerning the vertical line $t = \tau$ and its shape is only dependent of k_{YN}. The height decreases and the width increases with the decrease in k_{YN}. As mentioned above, τ is a location parameter and thereby affects the location of the breakthrough curve and rate profile alone. The effects of k_T (k_{BA}) and q_0 (a_0) on the breakthrough curve and rate profile are consistent with that of k_{YN} and τ, respectively because the Bohart–Adams, Thomas and Yoon–Nelson models are equivalent in mathematical nature.

In the Clark model, one can readily see from Figure 2-6 that the parameter n can affect the curvature and location of the breakthrough curve. It becomes steeper with the decrease in n. The rate profiles for different n exhibit three types: (i) A symmetric Gaussian distribution shape ($n = 2$); (ii) An asymmetric quasi-Gaussian distribution shape with a widened right-hand side ($1 < n < 2$); and (iii) An asymmetric quasi-Gaussian distribution shape with a widened left-hand side ($2 < n < 10$). As mentioned above, the Clark model can be converted to the Yoon–Nelson

model. Thus, the effects of the parameters A and r on the breakthrough curve and rate profile are equivalent to that of k_{YN} and τ, respectively.

In the dose-response model, the effects of the parameters a and b on the breakthrough curve and rete profile are represented in Figure 2-7. The influence of a on the breakthrough curve has been discussed in detail (vide supra). The corresponding rate profile is an asymmetric quasi-Gaussian distribution shape with a widened right-hand side (Figure 2-7c). The increase in a leads to the increased height and reduced width, while the location of the peak is shifted to the left side. It can be clearly seen from Figure 2-7b and Figure 2-7d that the breakthrough curves and rate profiles are shifted to the right side by a certain distance with the decrease in b. The curvature of the breakthrough curves and the maximum specific breakthrough rate μ_{max} also decrease correspondingly. The Bohart–Adams, Thomas, Yoon–Nelson, Clark and dose-response models represent different types of the breakthrough curves and rate profiles, which provide more flexible selection for the modeling of a continuous-flow fixed-bed column.

2.6. Physical meanings of characteristic parameters

In order to better understand the dynamic behaviors in a fixed-bed column, it is of prime importance to explain the physical meanings of model parameters correctly. In the Yoon–Nelson model, k_{YN} and τ are the rate constant independent of time and the operating time required to reach 50% breakthrough, respectively. Many studies indicate that the values of k_{YN} and τ are dependent of the operating conditions such as influent solute concentration, flow rate and bed height. Thus, both k_{YN} and τ are more likely to be the lumped constants that are related to the physical processes and operating features.

In the Bohart–Adams and Thomas models, k_{BA} and k_T are the rate constants independent of time. The physical meanings of a_0x/uc_0 and q_0m/vc_0 represent the operating time required to reach 50% breakthrough according to Eq. (2-5). The rate constant k_{BA} (k_T) and adsorption capacity a_0 (q_0) are also related to the physical processes and operating features. Moreover, the change in certain parameter of a_0x/uc_0 or q_0m/vc_0 without adjusting a_0x/uc_0 or q_0m/vc_0 does not alter adsorption performance. The most prominent advantage of using a_0x/uc_0 or q_0m/vc_0 consists in the fact that one can readily see which group of the parameters affects adsorption

performance rather than examining the effect of each parameter.

In the Clark model, the parameter n is the Freundlich constant, representing a measure of adsorption intensity (Carabineiro et al., 2011). Although the Clark model assumes that the adsorption process follows the Freundlich isotherm, the adsorption in a fixed-bed column differs from that in a batch reactor (Worch, 2012): In a batch reactor, the mass transfer driving force or the adsorption rate decreases due to the reduced concentration during the adsorption process, while the adsorbent in a fixed-bed column is always in contact with the influent concentration, resulting in a high driving force over the whole process. Thus, it is reasonable to directly calculate the parameter n instead of the n value obtained from the batch reactor when the Clark model is used to analyze the experimental data. Besides, the parameters A and r are given as (Clark, 1987):

$$A = \left(\frac{{c_0}^{n-1}}{{c_\mathrm{b}}^{n-1}} - 1 \right) \exp(r t_\mathrm{b}) \tag{2-42}$$

$$r = (n-1)(K_\mathrm{T}/U_0) v_\mathrm{m} \tag{2-43}$$

The parameter A is a dimensionless constant according to Eq. (2-42) and r is related to the mass-transfer coefficient K_T. As discussed above, the Clark model can be also converted to the Yoon–Nelson model. As a result, A is considered as a location parameter and r is regarded as the rate constant.

In the dose-response model, the operating time required to reach 50% breakthrough is exactly $1/b$, which is not related to the parameter a. As a consequence, the half-operating time t_{50} only depends on the parameter b. As depicted in Figure 2-5a and Figure 2-7a, the effects of k_YN and a on the breakthrough curve are similar. Thus, the parameter a is related to the rate constant. It is worth noting that these model parameters mentioned above are determined by the adsorption system itself, mainly depend on the affinity of the adsorbent for the adsorbate molecules and initial operating conditions.

2.7. Summary

The Bohart–Adams, Thomas and Yoon–Nelson models provide the identical breakthrough curve and rate profile. The Wolborska model does not represent a complete sigmoidal curve.

The maximum specific breakthrough rate μ_{max}, lag time λ, inflection point t_i and half-operating time t_{50} can better reflect mathematical characteristics of the breakthrough curve. The modified breakthrough models may be important alternative methods for analysis of continuous-flow adsorption system. The physical meanings of q_0m/vc_0 and a_0x/uc_0 are the operating time required to reach 50% breakthrough, respectively. The dose-response model represents a sigmoidal curve only when the parameter a is more than unity ($a > 1$).

Table 2-1 Breakthrough models and the corresponding modified models.

Name	Equation	Modified equation
Bohart–Adams	$\frac{c}{c_0}=\frac{1}{1+\exp\left[k_{\mathrm{BA}}c_0\left(\frac{a_0x}{uc_0}-t\right)\right]}$	$\frac{c}{c_0}=\frac{1}{1+\exp\left[4\mu_{\max}(\lambda-t)+2\right]}$
Thomas	$\frac{c}{c_0}=\frac{1}{1+\exp\left[k_{\mathrm{T}}c_0\left(\frac{q_0m}{vc_0}-t\right)\right]}$	$\frac{c}{c_0}=\frac{1}{1+\exp\left[4\mu_{\max}(\lambda-t)+2\right]}$
Yoon–Nelson	$\frac{c}{c_0}=\frac{1}{1+\exp[k_{\mathrm{YN}}(\tau-t)]}$	$\frac{c}{c_0}=\frac{1}{1+\exp\left[4\mu_{\max}(\lambda-t)+2\right]}$
Clark	$\frac{c}{c_0}=\frac{1}{[1+A\exp(-rt)]^{\frac{1}{n-1}}}$	$\frac{c}{c_0}=\frac{1}{\left\{1+(n-1)\cdot\exp\left[\mu_{\max}\cdot n^{\frac{n}{n-1}}(\lambda-t)+n\right]\right\}^{\frac{1}{n-1}}}$
Dose-response	$\frac{c}{c_0}=1-\frac{1}{1+(bt)^a}$	$\frac{c}{c_0}=1-\frac{1}{1+\left\{\frac{t}{\lambda}\left[\frac{\left(\lambda\mu_{\max}+\sqrt{1+\lambda\mu_{\max}}\right)^2-1}{\left(\lambda\mu_{\max}+\sqrt{1+\lambda\mu_{\max}}\right)^2+1}\right]^{1+\frac{1}{\left(\lambda\mu_{\max}+\sqrt{1+\lambda\mu_{\max}}\right)^2}}\right\}^{\left(\lambda\mu_{\max}+\sqrt{1+\lambda\mu_{\max}}\right)^2}}$
Wolborska	$\frac{c}{c_0}=\exp\left(\frac{\beta_{\mathrm{a}}c_0}{a_0}t-\frac{\beta_{\mathrm{a}}}{u}x\right)$	Non-existence

In the dose-response model, $b = vc_0/q_0m$.

Table 2-2 Mathematical relationships between model parameters and four parameters defined in this study.

Models	μ_{max}	λ	t_{50}	t_i
Bohart–Adams	$\frac{k_{BA}c_0}{4}$	$\frac{a_0 x}{uc_0} - \frac{2}{k_{BA}c_0}$	$\frac{a_0 x}{uc_0}$	$\frac{a_0 x}{uc_0}$
Thomas	$\frac{k_T c_0}{4}$	$\frac{q_0 m}{vc_0} - \frac{2}{k_T c_0}$	$\frac{q_0 m}{vc_0}$	$\frac{q_0 m}{vc_0}$
Yoon–Nelson	$\frac{k_{YN}}{4}$	$\tau - \frac{2}{k_{YN}}$	τ	τ
Clark	$r \cdot n^{-\frac{n}{n-1}}$	$-\frac{1}{r}\left[\ln\left(\frac{n-1}{A}\right) + n\right]$	$-\frac{1}{r}\ln\left(\frac{2^{n-1}-1}{A}\right)$	$-\frac{1}{r}\ln\left(\frac{n-1}{A}\right)$
Dose-response	$\frac{b}{4a} \cdot (a-1)^{\frac{a-1}{a}} \cdot (a+1)^{\frac{a+1}{a}}$	$\frac{1}{b}\left(\frac{a-1}{a+1}\right)^{\frac{a+1}{a}}$	$\frac{1}{b}$	$\frac{1}{b}\left(\frac{a-1}{a+1}\right)^{\frac{1}{a}}$

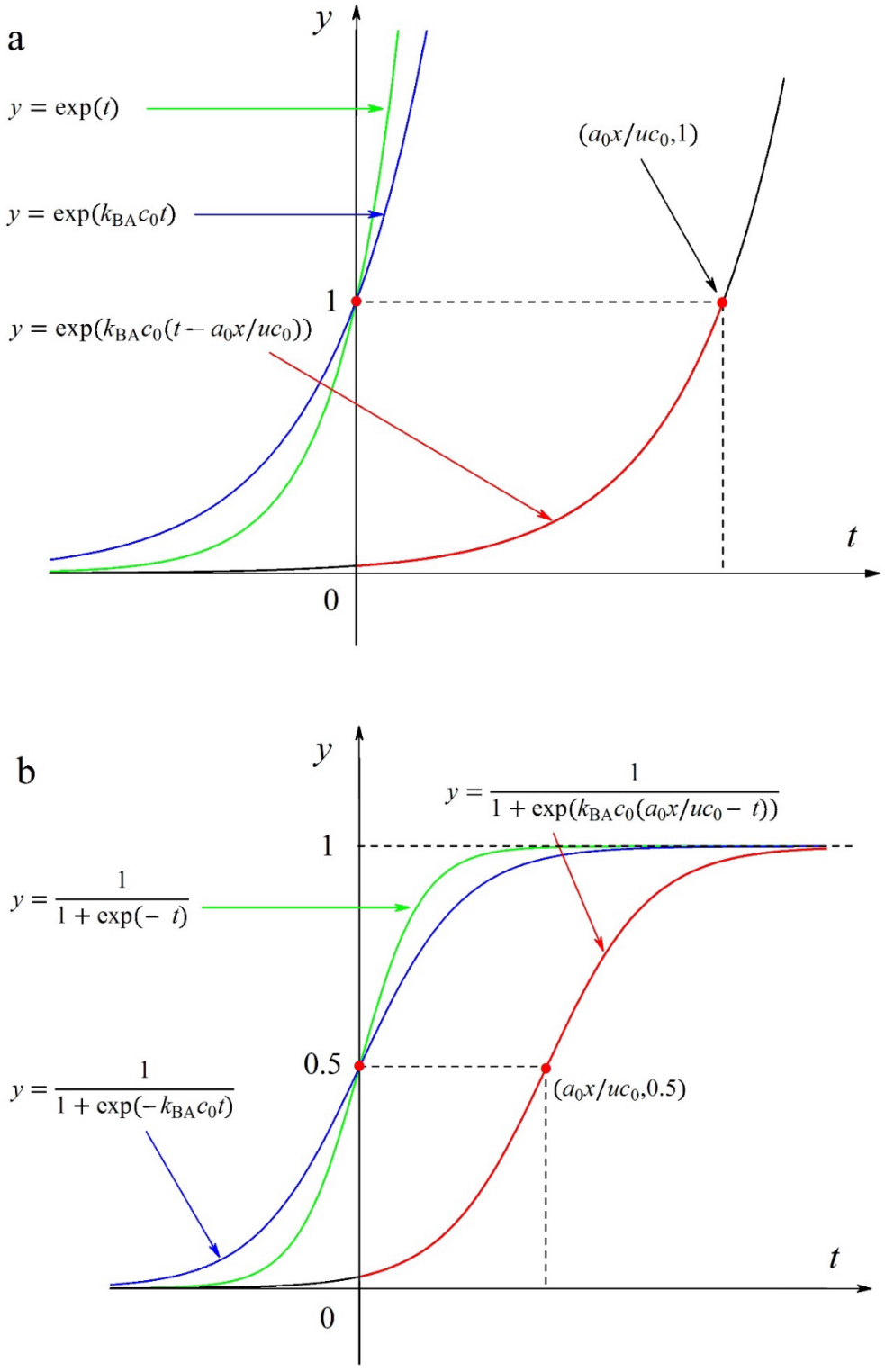

Figure 2-1 Schematic diagram of stretching and translation transformations for different forms of the Bohart–Adams model.

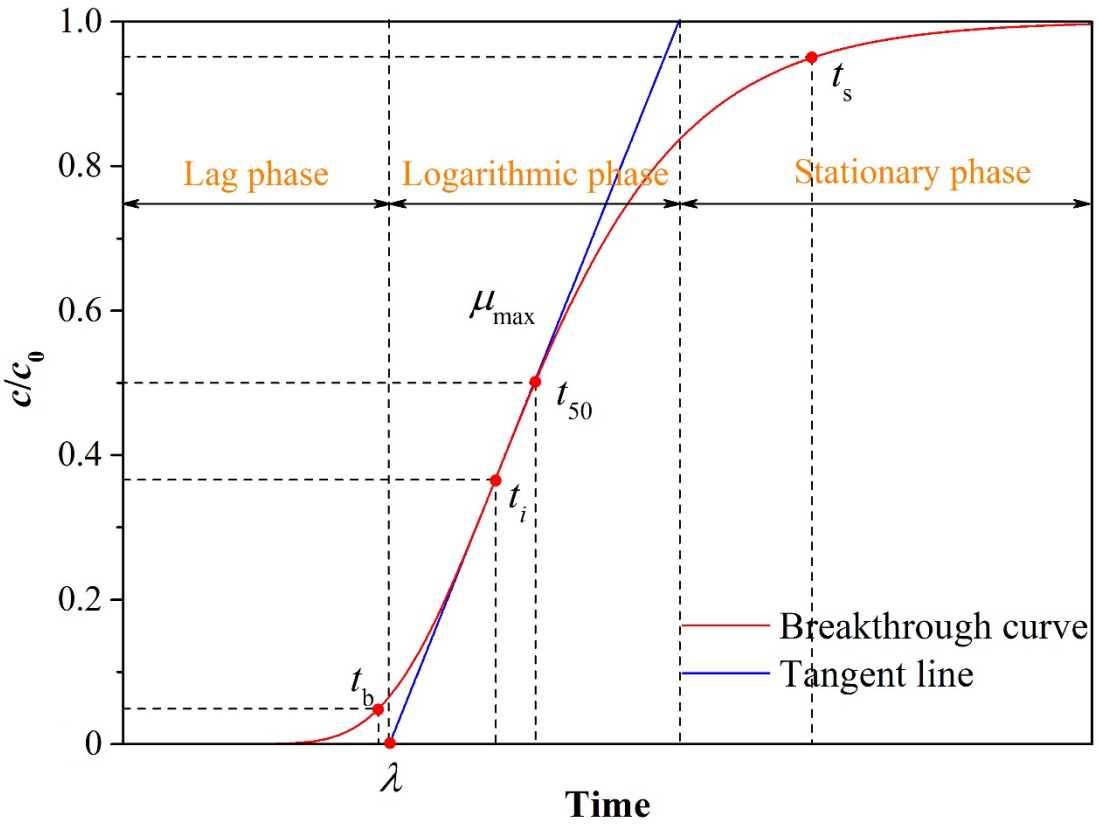

Figure 2-2 Schematic diagram of the breakthrough curve and the corresponding parameters.

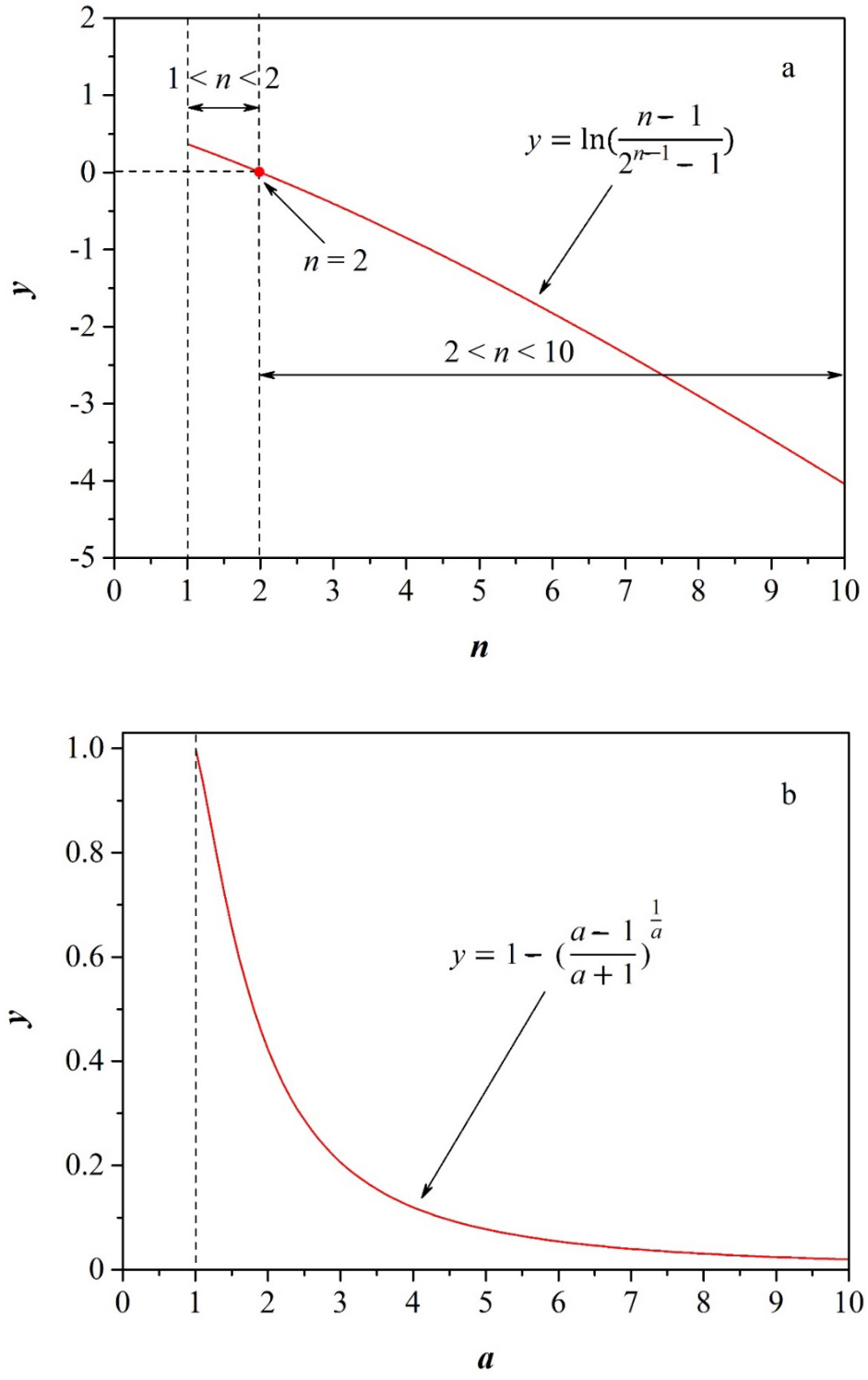

Figure 2-3 A plot of y as functions of parameters n and a for (a) Clark and (b) dose-response models ($y = t_{50} - t_i$).

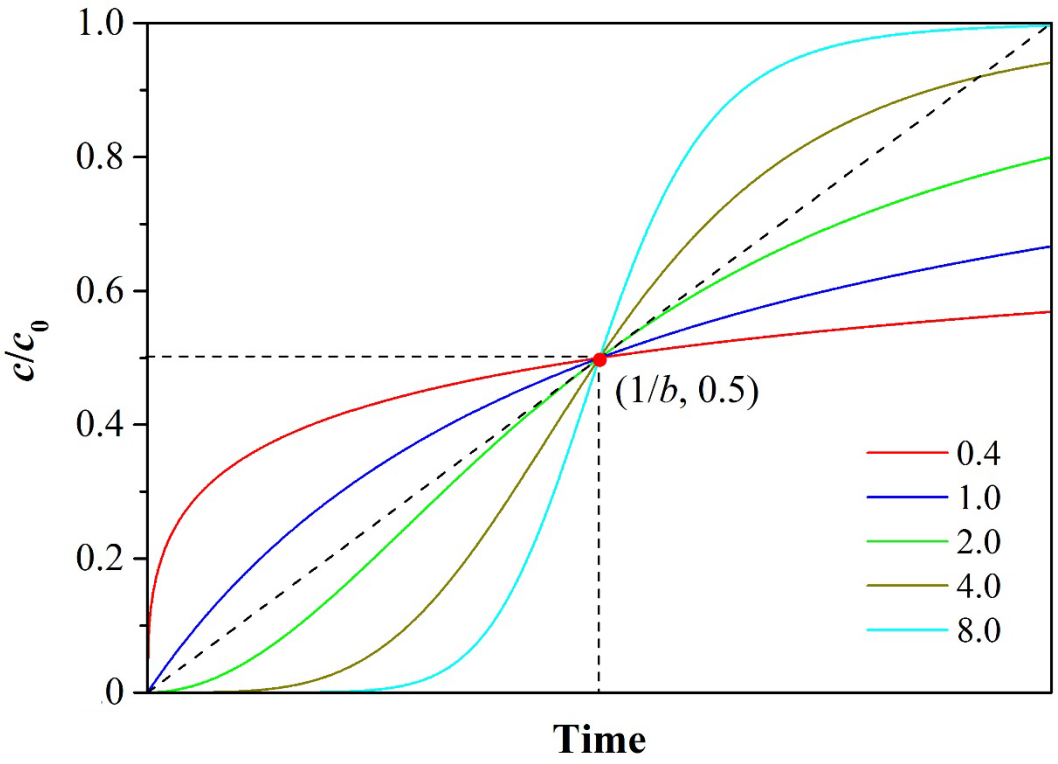

Figure 2-4 Effect of the parameter *a* on the breakthrough curve for the dose-response model.

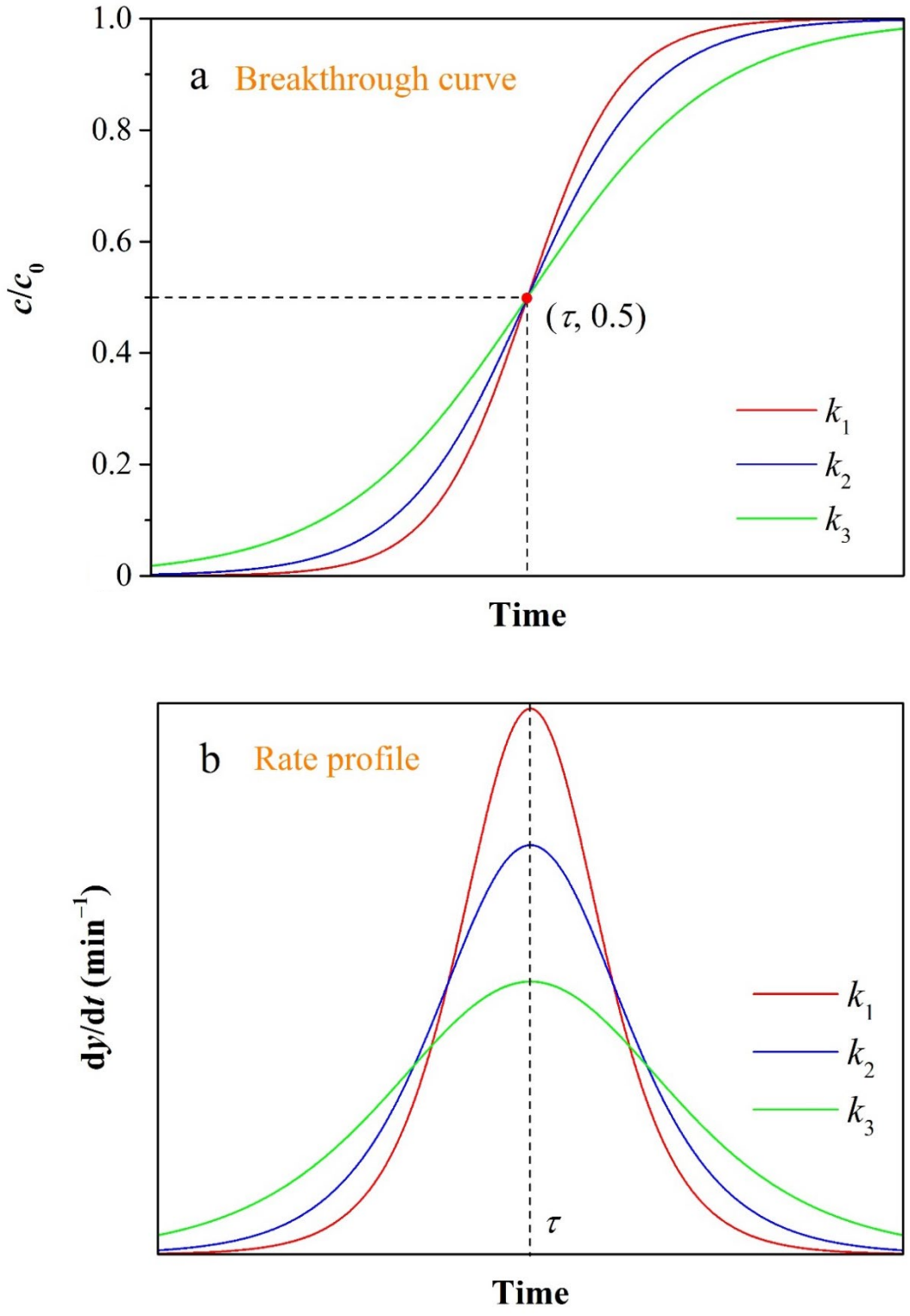

Figure 2-5 Effects of the rate constant on (a) breakthrough curve and (b) rate profile for the Yoon–Nelson model ($k_1 > k_2 > k_3$).

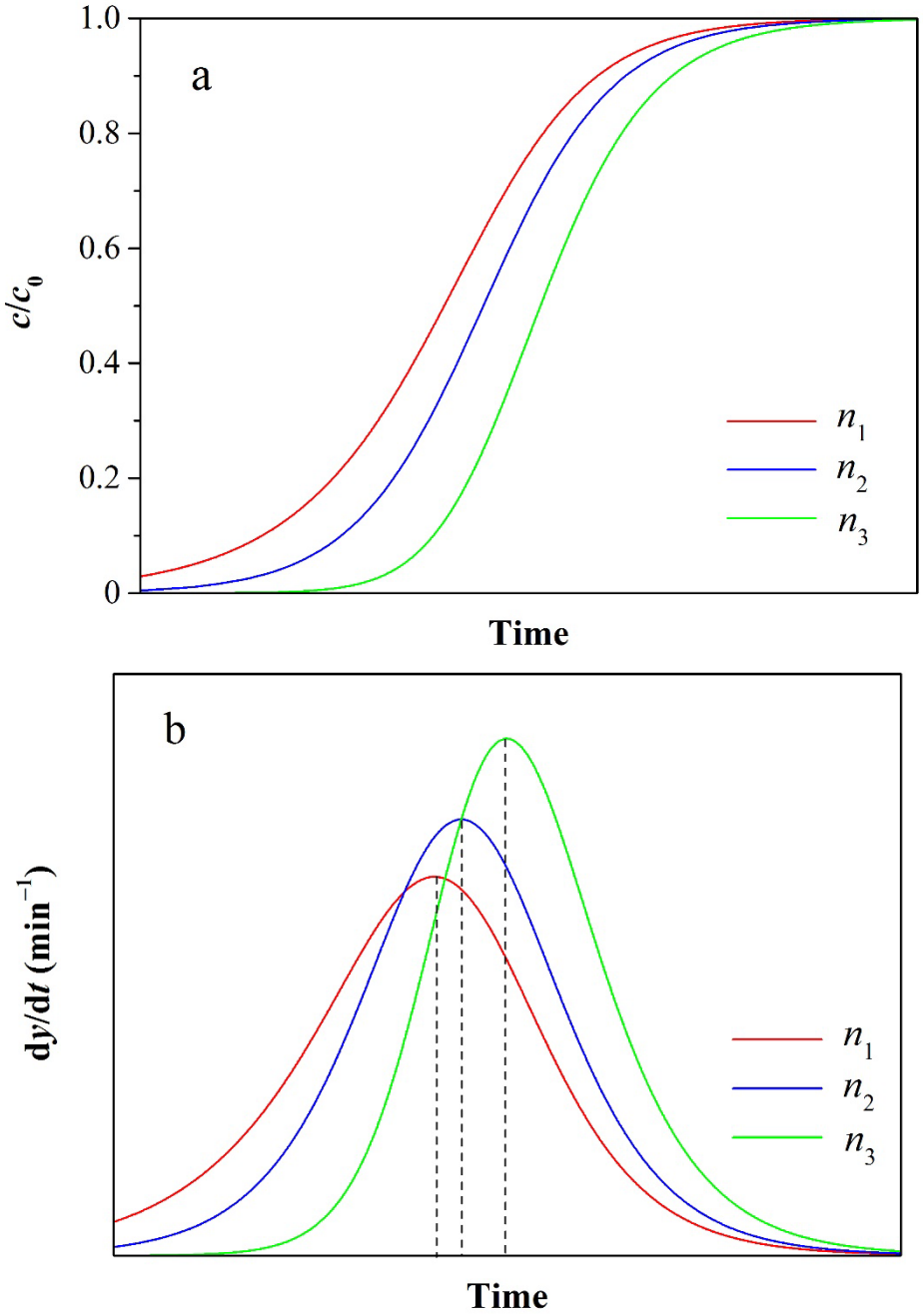

Figure 2-6 Effects of the parameter n on (a) breakthrough curve and (b) rate profile for the Clark model ($n_1 > n_2 > n_3$).

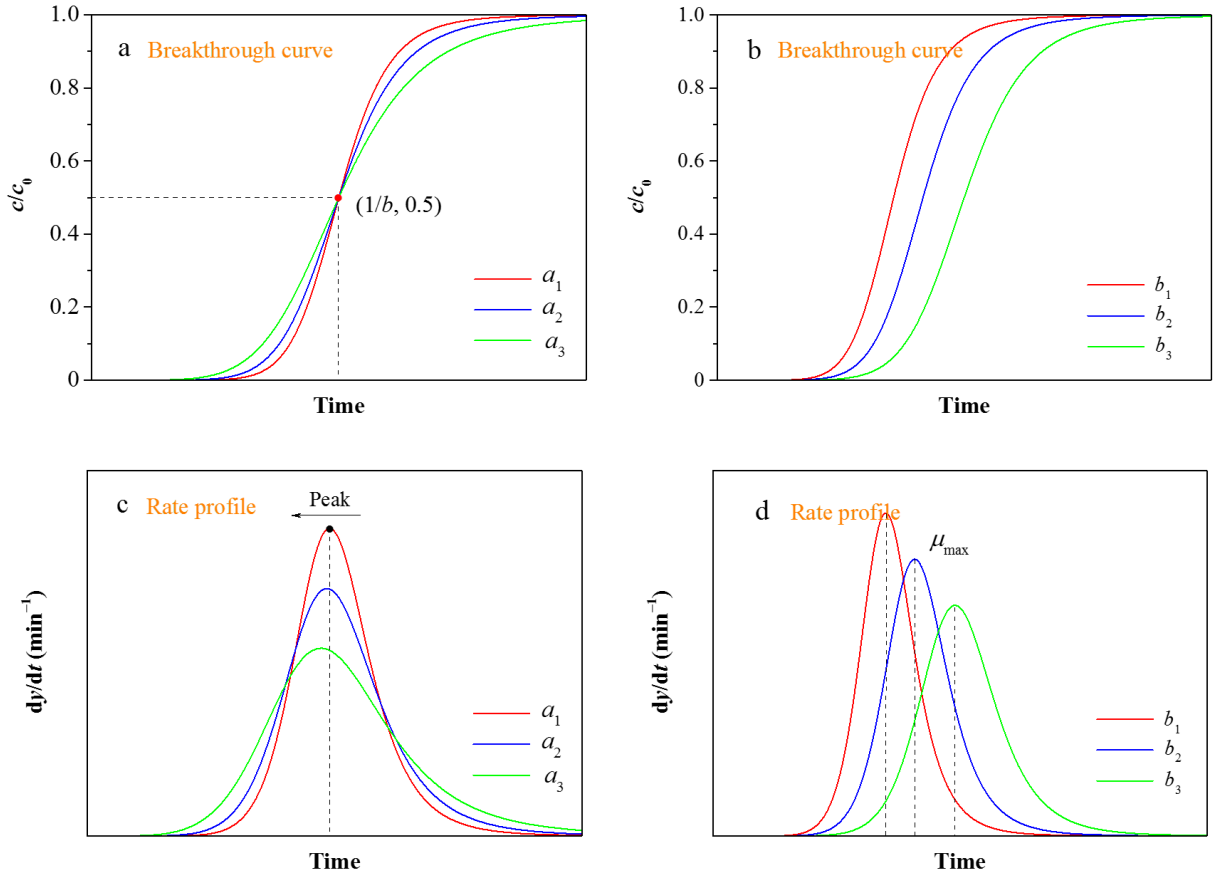

Figure 2-7 Effects of the parameters a and b on breakthrough curve and rate profile for the dose-response model ($a_1 > a_2 > a_3 > 1$ and $b_1 > b_2 > b_3$).

Chapter 3 Fractal-like kinetics of adsorption on heterogeneous surfaces in a fixed-bed column

3.1. Introduction

In order to gain insights into the dynamic behaviors in a fixed-bed column, the various breakthrough models have been proposed to describe the breakthrough curve under the specific operating condition. The most frequently used breakthrough models include the Bohart–Adams, Thomas and Yoon–Nelson models. The fitting curves provided by the three breakthrough models agree well with the experimental results under different experimental conditions such as influent solute concentration, flow rate, bed height, pH, temperature, adsorbent mass and particle size (Jang and Lee, 2016; Sheng et al., 2018; Witek-Krowiak et al., 2013). The three breakthrough models assume that the rate constant is independent of time.

However, when the reactants are spatially constrained by either walls, phase boundaries or force fields on the microscopic level, it is found to be unsatisfactory (Kopelman, 1988). It is expected that the adsorption process at the solid/solution interface is of high heterogeneity. The rate of adsorption for porous adsorbents is related not only to the reaction rate on the active sites, but also to the external mass transfer and intraparticle diffusion (Figaro et al., 2009). The classical reaction kinetics is not applicable for the heterogeneous diffusion-limited process (Montagnaro and Balsamo, 2014). It is reported that the adsorption kinetics at the solid/solution interface can be described by the fractal-like approach in a real system with different types of surface sites (Haerifar and Azizian, 2014). It is worth noting that the fractal-like concept is not been discussed in a fixed-bed adsorption system. Inspired by this, the fractal-like concept or time-dependent rate constant is introduced into the Bohart–Adams, Thomas and Yoon–Nelson models to obtain the corresponding fractal-like breakthrough models.

3.2. Theoretical analysis

In adsorption studies, some techniques such as surface protonation, chemical modification and thermal treatment are widely used to enhance the affinity and selectivity of the adsorbent, and thus most of the modified adsorbents have heterogeneous surfaces with different types of

adsorption sites (Loganathan et al., 2013). The interaction of energetic and geometric heterogeneity results in fractal-like kinetics (Kopelman, 1986). It represents a new insight into the adsorption behaviors at the solid/solution interface. The fractal-like adsorption kinetics indicates that the observed rate constant k is a time-dependent rate coefficient (Haerifar and Azizian, 2014; Kopelman, 1988), which can be expressed as:

$$k = k_0 t^{-h} \quad (0 \leq h \leq 1) \tag{3-1}$$

3.2.1. Fractal-like Bohart–Adams model

The Bohart–Adams model assumes that the adsorption reaction is not instantaneous and that the rate of the reaction is proportional to the residual adsorption capacity of the adsorbent and to the concentration of the adsorbate (Bohart and Adams, 1920). The decay rate of the concentration of the adsorbate in the outlet is given as:

$$\frac{\partial c}{\partial x} = -\frac{k_{\mathrm{BA}} a c}{u} \tag{3-2}$$

The decay rate of the residual adsorption capacity for a given amount of the adsorbent is given as:

$$\frac{\partial a}{\partial t} = -k_{\mathrm{BA}} a c \tag{3-3}$$

Substitution of Eq. (3-1) to Eq. (3-2) and Eq. (3-3) leads to

$$\frac{\partial c}{\partial x} = -\frac{k_{\mathrm{BA},0} t^{-h} a c}{u} \tag{3-4}$$

$$\frac{\partial a}{\partial t} = -k_{\mathrm{BA},0} t^{-h} a c \tag{3-5}$$

Let $a^* = a/a_0$, $c^* = c/c_0$, $x^* = k_{\mathrm{BA},0} t^{-h} a_0 x/u$ and $t^* = k_{\mathrm{BA},0} t^{-h} c_0 t$ (where a_0 (mg L^{-1}) is the initially available adsorption capacity of the adsorbent and c_0 (mg L^{-1}) is the concentration of the adsorbate in the inlet), then:

$$\frac{\partial c^*}{\partial x^*} = -a^* c^* \tag{3-6}$$

$$\frac{\partial a^*}{\partial t^*} = -a^* c^* \frac{t^{-h}}{1-h} \left(\frac{1}{k_{\mathrm{BA},0} c_0} t^* \right)^{\frac{h}{1-h}} \tag{3-7}$$

or

$$\frac{\partial \ln c^*}{\partial x^*} = -a^* \tag{3-8}$$

$$\frac{\partial \ln a^*}{\partial t^*} = -c^* \frac{t^{-h}}{1-h}\left(\frac{1}{k_{\mathrm{BA},0}c_0}t^*\right)^{\frac{h}{1-h}} \tag{3-9}$$

Integrating Eq. (3-8) and Eq. (3-9) at the boundary conditions of $t^*= 0$, $a^*= 1$ and $x^*= 0$, $c^*= 1$ leads to

$$c^* = \exp(-x^*) \tag{3-10}$$

$$a^* = \exp\left[-k_{\mathrm{BA},0}t^{-h}c_0\left(\frac{1}{k_{\mathrm{BA},0}c_0}t^*\right)^{\frac{1}{1-h}}\right] \tag{3-11}$$

Dividing Eq. (3-10) by Eq. (3-11) leads to

$$\frac{c^*}{a^*} = \exp\left[k_{\mathrm{BA},0}t^{-h}c_0\left(\frac{1}{k_{\mathrm{BA},0}c_0}t^*\right)^{\frac{1}{1-h}} - x^*\right] \tag{3-12}$$

Substitution of Eq. (3-12) into Eq. (3-6) leads to

$$\frac{-\frac{\partial c^*}{c^{*2}}}{\frac{\partial x^*}{}} = \frac{a^*}{c^*} = \exp\left[x^* - k_{\mathrm{BA},0}t^{-h}c_0\left(\frac{1}{k_{\mathrm{BA},0}c_0}t^*\right)^{\frac{1}{1-h}}\right] \tag{3-13}$$

Integrating Eq. (3-13) at the boundary condition of $x^*= 0$, $c^*= 1$ leads to

$$c^* = \frac{\exp\left[k_{\mathrm{BA},0}t^{-h}c_0\left(\frac{1}{k_{\mathrm{BA},0}c_0}t^*\right)^{\frac{1}{1-h}}\right]}{\exp\left[k_{\mathrm{BA},0}t^{-h}c_0\left(\frac{1}{k_{\mathrm{BA},0}c_0}t^*\right)^{\frac{1}{1-h}}\right] + \exp(x^*) - 1} \tag{3-14}$$

When the last term in the denominator is negligible. Eq. (3-14) reduces to

$$c^* = \frac{1}{1 + \exp\left[x^* - k_{\mathrm{BA},0}t^{-h}c_0\left(\frac{1}{k_{\mathrm{BA},0}c_0}t^*\right)^{\frac{1}{1-h}}\right]} \tag{3-15}$$

Substitution of $c^*= c/c_0$, $x^*= k_{\mathrm{BA},0}t^{-h}a_0x/u$ and $t^*= k_{\mathrm{BA},0}t^{-h}c_0t$ into Eq. (3-15) leads to

$$\frac{c}{c_0} = \frac{1}{1 + \exp\left[k_{\mathrm{BA},0}t^{-h}c_0\left(\frac{a_0x}{uc_0} - t\right)\right]} \tag{3-16}$$

3.2.2. Fractal-like Yoon–Nelson model

The Yoon–Nelson model assumes that the rate of decrease in the probability of adsorption

for each molecule is proportional to the probability of adsorption and the probability of breakthrough (Yoon and Nelson, 1984), which is expressed as:

$$-\frac{\mathrm{d}Q}{\mathrm{d}t} = k_{\mathrm{YN}}QP \tag{3-17}$$

where Q is the probability of adsorption ($Q = 1 - P$); P is the probability of breakthrough ($P = c/c_0$); k_{YN} (min^{-1}) is the Yoon–Nelson rate constant independent of time.

Substitution of Eq. (3-1) to Eq. (3-17) leads to

$$-\frac{\mathrm{d}Q}{\mathrm{d}t} = k_{\mathrm{YN},0}t^{-h}QP \tag{3-18}$$

After separation of variables, Eq. (3-18) is rewritten as:

$$\frac{\mathrm{d}Q}{Q(1-Q)} = -k_{\mathrm{YN},0}t^{-h}\mathrm{d}t \tag{3-19}$$

Integrating Eq. (3-19) at the boundary condition of $Q = 0.5$ at $t = \tau$ leads to

$$\ln\frac{Q}{(1-Q)} = \frac{k_{\mathrm{YN},0}}{1-h}\left(\tau^{(1-h)} - t^{(1-h)}\right) \tag{3-20}$$

or

$$\ln\frac{1-P}{P} = \frac{k_{\mathrm{YN},0}}{1-h}\left(\tau^{(1-h)} - t^{(1-h)}\right) \tag{3-21}$$

Substitution of $P = c/c_0$ into Eq. (3-21) leads to

$$\frac{c}{c_0} = \frac{1}{1+\exp\left(\frac{k_{\mathrm{YN},0}}{1-h}\left(\tau^{(1-h)} - t^{(1-h)}\right)\right)} \tag{3-22}$$

3.2.3. Fractal-like Thomas models

The Thomas model is widely used to estimate the adsorption capacity and rate constant in a fixed-bed adsorption system. In Chapter 1, it has been demonstrated that the Bohart–Adams and Thomas models are mathematically identical and have interchangeable parameters (Chu, 2010). In fact, the Bohart–Adams model is based on the bed height, while the Thomas model is based on the adsorbent mass. Herein, the fractal-like Thomas model is written as:

$$\frac{c}{c_0} = \frac{1}{1+\exp\left[k_{\mathrm{T},0}t^{-h}c_0\left(\frac{q_0 m}{vc_0} - t\right)\right]} \tag{3-23}$$

3.3. Materials and methods

3.3.1. Materials

All chemicals used in this study were of analytical grade without further purification. Chitosan (Deacetylation degree = max. 80%; Viscosity = 20–100 mPa·s) was purchased from Tokyo Chemical Industry Co., Ltd., Japan. Acetic acid, ferric chloride ($FeCl_3$), ammonia solution, hydrochloric acid, potassium nitrate (KNO_3) and sulphamic acid were provided by Wako Pure Chemical Industries, Ltd, Japan. A certain amount of KNO_3 was dissolved into deionized water to prepare 50 mg L^{-1} (as NO_3^--N) nitrate solution.

3.3.2. Adsorbent preparation

6 g of chitosan powders were added to a beaker containing 300 mL of deionized water, followed by addition of 10 mL of acetic acid. The mixture solution was consecutively stirred by a magnetic stirrer for 2.0 h at room temperature. A certain amount of $FeCl_3$ was added to the mixture solution until uniform solution appeared. The resultant solution was dropwise added into ammonia solution (approximately 8%) using a disposable syringe. The obtained spherical hydrogel beads were stabilized for 1.0 h, and then these hydrogel beads were sufficiently washed with deionized water to remove surface residuals and were dried in an oven at 55 °C. Next, the dried beads were soaked in a certain amount of deionized water for 2.0 h. Finally, chitosan-Fe(III) composite was obtained through separation, washing and drying at the same condition and then stored in sealed plastic bag for further study.

3.3.3. Fixed-bed adsorption

Figure 3-1 shows a set-up diagram of nitrate adsorption in a continuous fixed-bed column system. The fixed-bed column was made of Pyrex glass tube with an inner diameter of 0.7 cm and a length of 60 cm. 3 g of chitosan-Fe(III) were packed in the column to yield the desired bed height (44 cm). The gauze was kept at the top and bottom of the column to stabilize the adsorbent and provide a uniform flow. The nitrate solution (50 mg L^{-1}) was fed into the column from the bottom by a peristaltic pump at 6.1 mL min^{-1}. The nitrate solution at the outlet of the column was collected at preset time intervals and the concentration of nitrate was measured by the ultraviolet spectrophotometry using a UV/vis spectrophotometer (UV–1800, Shimadzu, Japan).

3.4. Results and discussion

3.4.1. Error equations

The accurate estimation of the model parameters is very important to understand the breakthrough behaviors in a fixed-bed column. Error equations are statistics that quantify the error obtained from the correlation of experimental data by a mathematical model. The errors and model parameters can be determined by an iterative nonlinear regression (Alberti et al., 2012). The linearization of the nonlinear equations may change the error distributions and violate some of the assumptions behind regression analysis (Ahmed and Hameed, 2018). Therefore, in this study, the nonlinear curve fitting is used to address all experimental data by Origin 9 software (OriginLab Corp., USA). The reliability of the fractal-like breakthrough models is validated by the adjusted determination factor (Adj. R^2) (Hossein-Zadeh, 2015) and the reduced chi-squared value (χ^2) (Ramos et al., 2016). The larger Adj. R^2 and smaller χ^2 values show better fitting performance, which can be expressed as:

$$\text{Adj. } R^2 = 1 - \left(1 - R^2\right)\left(\frac{n-1}{n-p}\right) \tag{3-24}$$

$$\chi^2 = \frac{1}{f}\sum_{i=1}^{n} \omega_i \left(y_{\text{exp}} - y_{\text{cal}}\right)^2 \tag{3-25}$$

3.4.2. Fitting performance of fractal-like breakthrough models

The Bohart–Adams, Thomas, Yoon–Nelson models and corresponding fractal-like breakthrough models are listed in Table 3-1. It is predicted that the three fractal-like breakthrough models should have better fitting performance due to the introduction of an extra adjustable parameter h. As mentioned above, the Bohart–Adams and Thomas models, and fractal-like Bohart–Adams and fractal-like Thomas models are equivalent in mathematical nature. The conclusions with respect to the Bohart–Adams and fractal-like Bohart–Adams models are also applied to the Thomas and fractal-like Thomas models. In other words, the fractal-like Bohart–Adams and fractal-like Thomas models represent the same breakthrough curve and rate profile. Herein, in order to report this study concisely, the Thomas and fractal-like Thomas models are no longer further discussed.

In this study, the adsorption of nitrate on chitosan-Fe(III) composite was used to evaluate the applicability of the fractal-like breakthrough models. It can be clearly seen from Figure 3-2

that the fitting curves provided by the fractal-like Bohart–Adams and fractal-like Yoon–Nelson models pass through all experimental data points with few deviations and that the predicted values agree well with the observed values. Moreover, as shown in Table 3-2, compared with Bohart–Adams model, the fractal-like Bohart–Adams model has larger adjusted determination factor (Adj. R^2 = 0.9989) and smaller reduced chi-squared value ($\chi^2 = 1.25 \times 10^{-4}$), indicating that the fractal-like Bohart–Adams model is superior to the Bohart–Adams model. Similarly, the fractal-like Yoon–Nelson model also have larger Adj. R^2 and smaller χ^2 values (Adj. R^2 = 0.9992 and $\chi^2 = 8.86 \times 10^{-5}$). Therefore, the fractal-like Yoon–Nelson model has better fitting performance than the Yoon–Nelson model. In summary, the introduction of the fractal-like concept remarkably improves the fitting performance of the Bohart–Adams, Thomas and Yoon–Nelson models.

3.4.3. Rate profile

To date, more attention has been paid to the accurate determination of model parameters and error equations when the curve fitting is performed. In order to better understand the mass transfer process, it is essential to investigate the rate equations of Bohart–Adams, Thomas and Yoon–Nelson models and corresponding fractal-like models. The rate equations can be obtained by the first derivation of the fractal-like Bohart–Adams, fractal-like Thomas and fractal-like Yoon–Nelson models.

$$\frac{\mathrm{d}(c/c_0)}{\mathrm{d}t} = \frac{k_{\mathrm{BA},0}t^{-h}c_0\left[1 + ht^{-1}\left(\frac{a_0x}{uc_0} - t\right)\right] \cdot \exp\left[k_{\mathrm{BA},0}t^{-h}c_0\left(\frac{a_0x}{uc_0} - t\right)\right]}{\left\{1 + \exp\left[k_{\mathrm{BA},0}t^{-h}c_0\left(\frac{a_0x}{uc_0} - t\right)\right]\right\}^2} \tag{3-26}$$

$$\frac{\mathrm{d}(c/c_0)}{\mathrm{d}t} = \frac{k_{\mathrm{T},0}t^{-h}c_0\left[1 + ht^{-1}\left(\frac{q_0m}{vc_0} - t\right)\right] \cdot \exp\left[k_{\mathrm{T},0}t^{-h}c_0\left(\frac{q_0m}{vc_0} - t\right)\right]}{\left\{1 + \exp\left[k_{\mathrm{T},0}t^{-h}c_0\left(\frac{q_0m}{vc_0} - t\right)\right]\right\}^2} \tag{3-27}$$

$$\frac{\mathrm{d}(c/c_0)}{\mathrm{d}t} = \frac{k_{\mathrm{YN},0}t^{-h} \cdot \exp\left[\frac{k_{\mathrm{YN},0}}{1-h}\left(\tau^{(1-h)} - t^{(1-h)}\right)\right]}{\left\{1 + \exp\left[\frac{k_{\mathrm{YN},0}}{1-h}\left(\tau^{(1-h)} - t^{(1-h)}\right)\right]\right\}^2} \tag{3-28}$$

It should be noted that the rate profiles of the Bohart–Adams, Thomas and Yoon–Nelson models are coincident due to the fact that the three breakthrough models represent the same breakthrough curve. Moreover, the fractal-like Bohart–Adams and fractal-like Thomas models

also have the same rate profile.

It is commonly accepted that the adsorption process can be usually characterized by four consecutive steps: bulk transport, film diffusion, intraparticle diffusion and adsorptive attachment (Weber Jr, 1984), in which bulk transport and adsorption reaction can be fast accomplished, while film diffusion and intraparticle diffusion proceed slowly (Machado et al., 2011). As shown in Figure 3-3, the rate profile consists of four stages: slow increase (I), fast increase (II), fast decrease (III) and slow decrease (IV). This behavior may be explained by the following considerations according to the mass transfer processes mentioned above: In stage I, the bulk transport occurs rapidly when the influent passes through a fixed-bed column. Large numbers of the solutes are transferred from bulk solution to the solid/solution surface and fast react with adsorption sites on the adsorbent surface, leading to the low effluent concentration and thus the breakthrough rate increases slowly with time. In stage II, as the adsorption progresses, the number of available adsorption sites on the adsorbent surface reduces gradually and the mass transfer resistance increases due to the decrease in concentration gradient at the solid/solution interface, resulting in the rapid increase in the breakthrough rate; Before stage III, it is secondary for the adsorption of the solutes on the internal surface of the adsorbent caused by intraparticle diffusion. As the adsorption further proceeds, the adsorption of the solutes on the external surface reduces, while the porous adsorbent can still hold the solutes continuously due to the intraparticle diffusion. The mass transfer mechanism is converted from film diffusion to intraparticle diffusion. Thus, the breakthrough rate decreases rapidly because of intraparticle diffusion; In stage IV, the breakthrough rate approaches zero when all adsorption sites of the porous adsorbent approximate to the saturation.

3.4.4. Effect of fractal-like exponent *h* on breakthrough curve and rate profile

The effects of the parameter h on the breakthrough curves and rate profiles are described in Figure 3-4. According to Eq. (3-16) and Eq. (3-22), the operating times required to reach 50% breakthrough are exactly equivalent to a_0x/uc_0 and τ for the fractal-like Bohart–Adams and fractal-like Yoon–Nelson models, respectively regardless of the h values. Thus, all of the breakthrough curves will pass through one point for different h values. The breakthrough curves are stepper with the decrease in h. The shape of the breakthrough curves will become

asymmetric due to the introduction of the fractal-like exponent *h* and the trend of asymmetry is more distinct with the increase in *h*. As shown in Figure 3-4b and Figure 3-4d, the peak location of the rate profiles progressively shifts to the left with the increase in *h*. The introduction of the fractal-like exponent *h* makes the breakthrough curves and rate profiles asymmetric. Thus, the fractal-like Bohart–Adams, fractal-like Thomas and fractal-like Yoon–Nelson models can describe adsorption systems with asymmetric breakthrough curves.

3.4.5. Practical significance

In general, the shape of the breakthrough curve is determined by that of the adsorption isotherm and is affected by the respective transport process in the column and in the adsorbent (Chu, 2004). If the intraparticle diffusion is the rate-controlling step, the breakthrough curve will be asymmetric (Worch, 2012). Besides, if the adsorption rate falls off more rapidly than the residual adsorption capacity of the adsorbent or the adsorbent consists of two or more constituents of unequal reactivity, the breakthrough curve is also asymmetric (Bohart and Adams, 1920). Thus, in a fixed-bed adsorption system, the breakthrough curve is usually asymmetric in the adsorption of water pollutants even for adsorption of individual solute (Rojas-Mayorga et al., 2015). Although the Bohart–Adams, Thomas and Yoon–Nelson models can well describe many fixed-bed adsorption systems, the three breakthrough models are not suitable to describe the experimental data with asymmetric distribution. The introduction of the fractal-like concept significantly improves fitting performance and the symmetry of the breakthrough curves and rate profiles are only dependent of the fractal-like exponent *h*. Since the Bohart–Adams, Thomas and Yoon–Nelson models can be regarded as special cases of the corresponding fractal-like models ($h = 0$), the fractal-like Bohart–Adams, fractal-like Thomas and fractal-like Yoon–Nelson models have more extensive application. Furthermore, the reasonable explanation of the rate profiles contributes to better understanding mass transfer behaviors in a fixed-bed column. The significance of this study is to provide new alternative models for analyzing the column adsorption data and to further understand the adsorption rate and mass transfer process. In recent years, most of the adsorption studies focus on the synthesis of various novel adsorption materials. The main purposes of these studies are to select optimal model and obtain model parameters when the curve fitting is conducted. Little attention has

been paid to the development of the breakthrough models. The fractal-like Bohart–Adams, fractal-like Thomas and fractal-like Yoon–Nelson models proposed in this study is an important supplement of the adsorption kinetics.

3.5. Summary

The fractal-like Bohart–Adams, fractal-like Thomas and fractal-like Yoon–Nelson models with larger Adj. R^2 and smaller χ^2 values can more accurately describe nitrate adsorption on chitosan-Fe(III) composite. Introduction of the fractal-like concept results in the asymmetry of the breakthrough curve and rate profile. The shape of the rate profiles is similar to the Gaussian distribution shape. The mass transfer mechanism is converted from film diffusion to intraparticle diffusion at peak location of the rate profile. The decrease in the fractal-like exponent h leads to the stepper breakthrough curves and rapid adsorption rate. The fractal-like breakthrough models may be an alternative method for the analysis of fixed-bed adsorption systems.

Table 3-1 Bohart–Adams, Thomas and Yoon–Nelson models and the corresponding fractal-like models.

Models	Equations	Fractal-like equations
Bohart–Adams	$\frac{c}{c_0}=\frac{1}{1+\exp\left[k_{\mathrm{BA}}c_0\left(\frac{a_0x}{uc_0}-t\right)\right]}$	$\frac{c}{c_0}=\frac{1}{1+\exp\left[k_{\mathrm{BA},0}t^{-h}c_0\left(\frac{a_0x}{uc_0}-t\right)\right]}$
Thomas	$\frac{c}{c_0}=\frac{1}{1+\exp\left[k_{\mathrm{T}}c_0\left(\frac{q_0m}{vc_0}-t\right)\right]}$	$\frac{c}{c_0}=\frac{1}{1+\exp\left[k_{\mathrm{T},0}t^{-h}c_0\left(\frac{q_0m}{vc_0}-t\right)\right]}$
Yoon–Nelson	$\frac{c}{c_0}=\frac{1}{1+\exp[k_{\mathrm{YN}}(\tau-t)]}$	$\frac{c}{c_0}=\frac{1}{1+\exp\left[\frac{k_{\mathrm{YN},0}}{1-h}\left(\tau^{(1-h)}-t^{(1-h)}\right)\right]}$

Table 3-2 Parameters and errors obtained from the Bohart–Adams and Yoon–Nelson models and corresponding fractal-like models.

Bohart–Adams				Fractal-like Bohart–Adams				
k_{BA} (L mg^{-1} min^{-1})	a_0 (mg L^{-1})	χ^2	Adj. R^2	$k_{BA,0}$ (L mg^{-1} min$^{-(1-h)}$)	a_0 (mg L^{-1})	h	χ^2	Adj. R^2
3.09×10^{-4}	2942.3	1.37×10^{-3}	0.9878	1.66×10^{-3}	2742.3	0.339	1.25×10^{-4}	0.9989
Yoon–Nelson				Fractal-like Yoon–Nelson				
k_{YN} (min^{-1})	τ (min)	χ^2	Adj. R^2	$k_{YN,0}$ (min$^{-(1-h)}$)	τ (min)	h	χ^2	Adj. R^2
1.54×10^{-2}	163.4	1.37×10^{-3}	0.9878	0.498	152.3	0.690	8.86×10^{-5}	0.9992

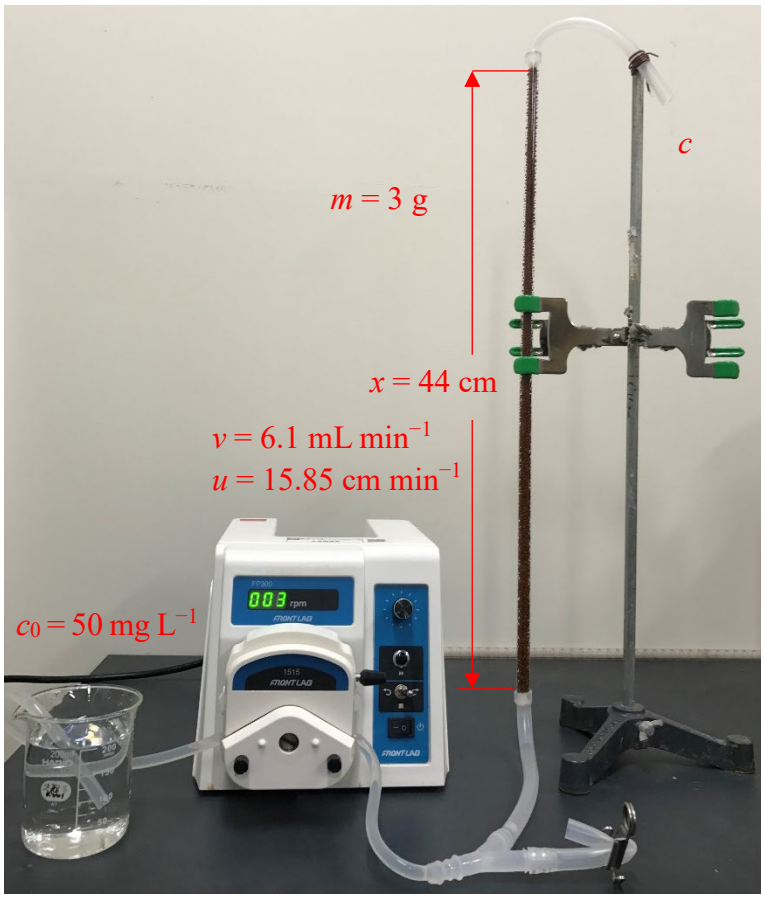

Figure 3-1 Set-up diagram of nitrate adsorption in a continuous-flow system.

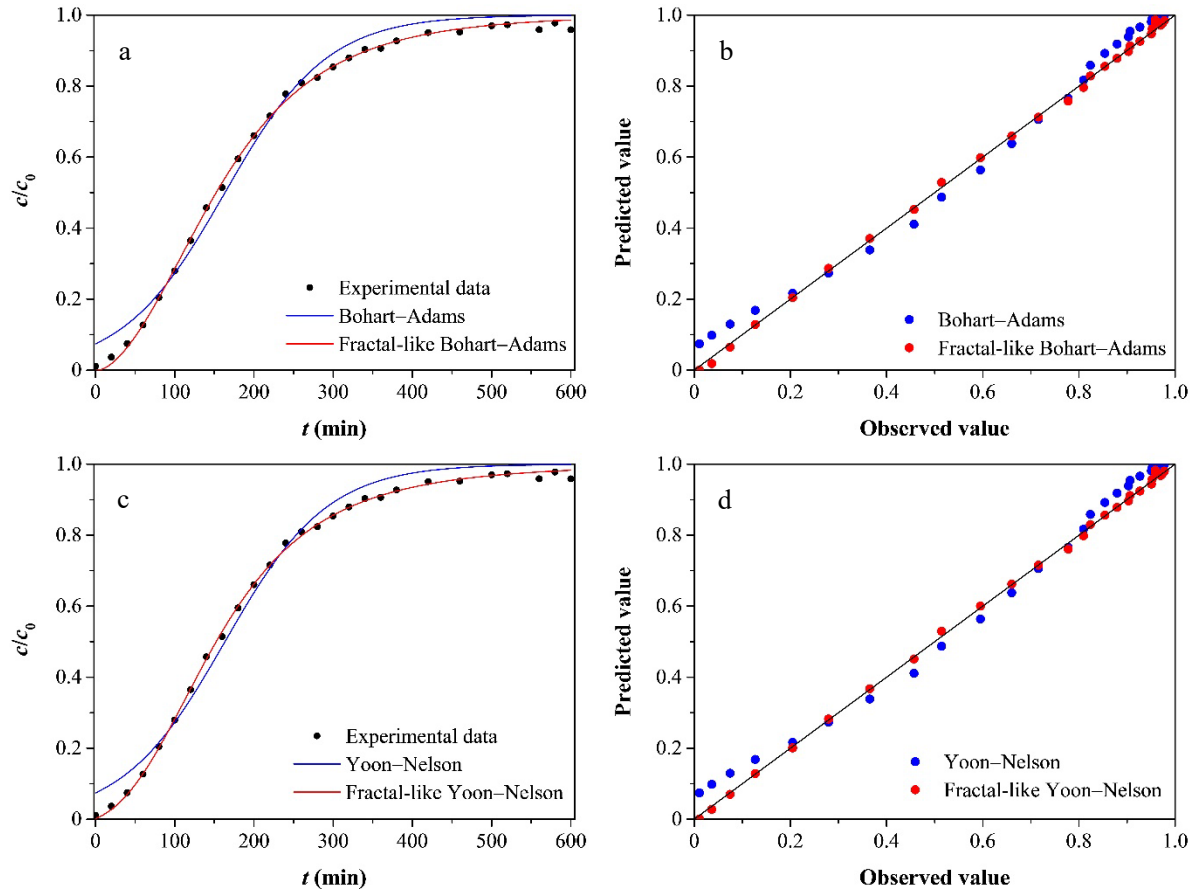

Figure 3-2 Modeling of nitrate adsorption on chitosan-Fe(III) composite using Bohart–Adams, Yoon–Nelson, fractal-like Bohart–Adams and fractal-like Yoon–Nelson models: (a and c) breakthrough curve and (b and d) predicted versus observed values.

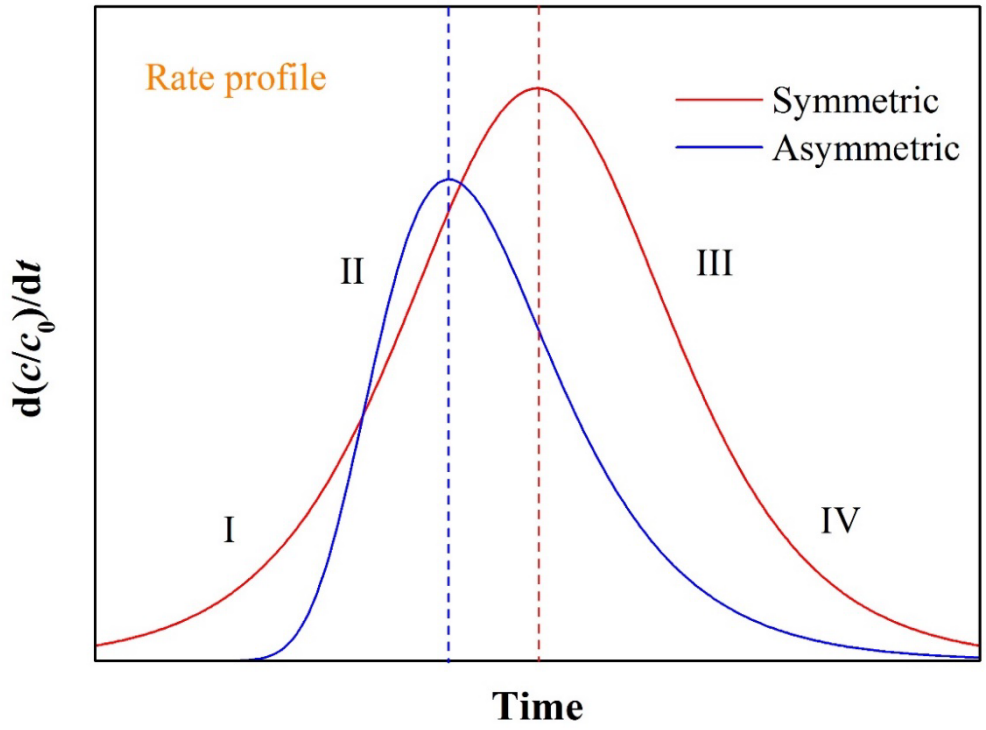

Figure 3-3 Schematic diagram of the rate profiles for different rate constants.

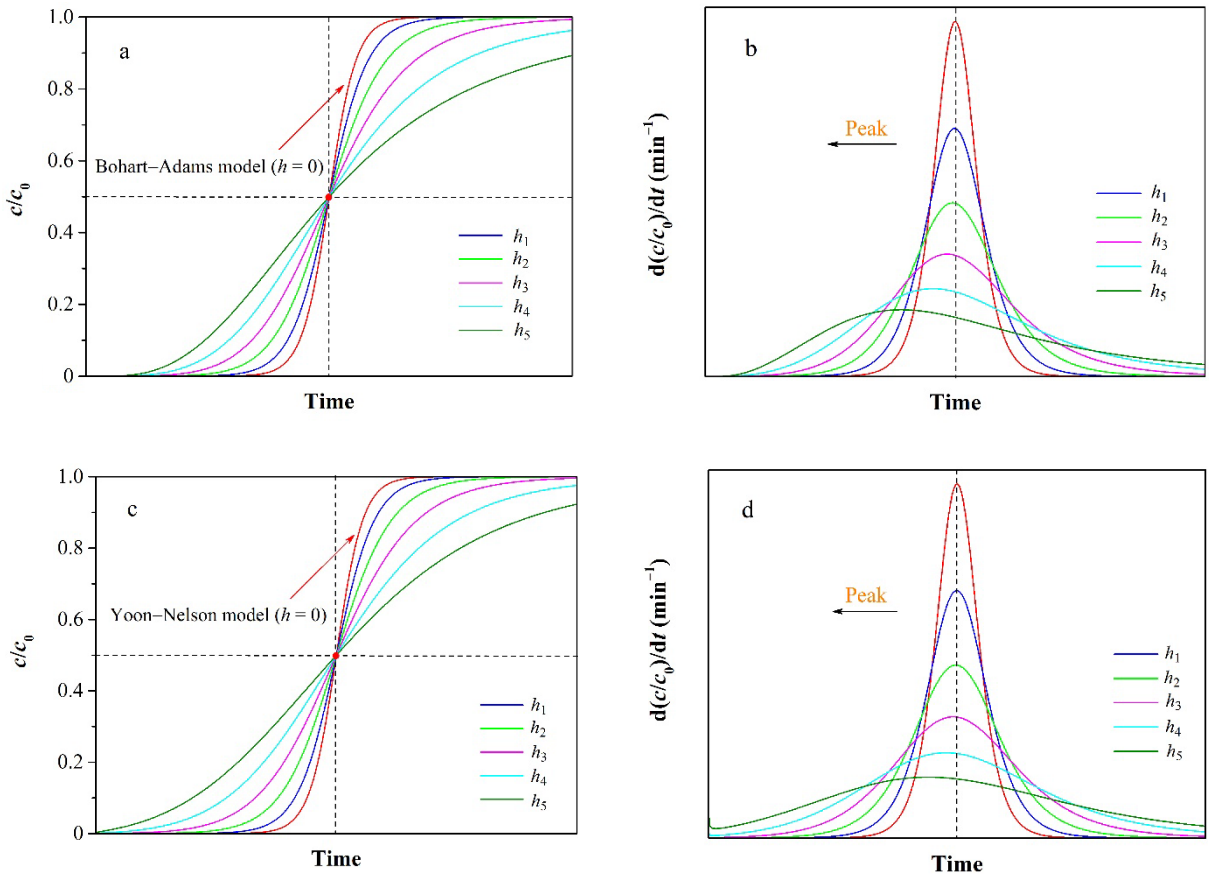

Figure 3-4 Schematic diagram for the effects of the fractal-like exponent h on (a and c) breakthrough curves and (b and d) rate profiles for different h values ($0 < h_1 < h_2 < h_3 < h_4 < h_5 < 1$).

Chapter 4 Prediction of breakthrough behaviors using hyperbolic tangent and double exponential models in a fixed-bed column

4.1. Introduction

In order to more accurately describe the breakthrough behaviors in a fixed-bed column, the use of simple and tractable equations that avoid the need for numerical solution is likely to be more suitable and logical (Chu, 2004). Many attempts have been made to describe the breakthrough behaviors in a fixed-bed column and several theoretical and empirical models have been proposed for this purpose. The most widely used breakthrough models include the Bohart–Adams, Thomas and Yoon–Nelson models. The distribution of the experimental data often varies considerably for different adsorbent-adsorbate systems. The three breakthrough models only represent symmetric breakthrough curves and thus are not likely to adapt to all adsorption systems. In other words, the Bohart–Adams, Thomas and Yoon–Nelson models fail to describe asymmetric breakthrough curves well. Thus, developing some new breakthrough models may contribute to the description of more adsorption systems and the acquisition of more reliable parameters. Moreover, the traditional breakthrough models mainly focus on adsorption capacity and ignore the change in the adsorption rate during the adsorption processes. In this chapter, the mathematical relationships between model parameters (k, τ and n) and four parameters defined in Chapter 2 (μ_{max}, λ, t_i and t_{50}) are also further discussed.

This study mainly focuses on the establishment of the new breakthrough models and the more complete description of the breakthrough curves. The new breakthrough models are established on the basis of to the hyperbolic tangent and double exponential functions. Introduction of the parameter n into the new breakthrough models leads to the corresponding modified breakthrough models. The mathematical characteristics of the breakthrough curves and rate profiles are also discussed in detail.

4.2. Theoretical analysis

4.2.1. Mathematical characteristics of sigmoidal functions

The sigmoidal functions considered in this study include the hyperbolic tangent and double

exponential functions. In order to establish empirical breakthrough models, it is necessary to understand mathematical characteristics of the two functions at first.

(1) Hyperbolic tangent function

The hyperbolic tangent function is expressed as:

$$y = \tanh(x) \tag{4-1}$$

The first and second derivatives of Eq. (4-1) with respect to x are given as:

$$\frac{\mathrm{d}y}{\mathrm{d}x} = 1 - \tanh^2(x) \tag{4-2}$$

$$\frac{\mathrm{d}^2y}{\mathrm{d}x^2} = -2\tanh(x) \cdot [1 - \tanh^2(x))] \tag{4-3}$$

The second derivative is equal to zero at the inflection point $x = x_i$.

$$\left.\frac{\mathrm{d}^2y}{\mathrm{d}x^2}\right|_{x=x_i} = 0 \Longrightarrow x_i = 0 \tag{4-4}$$

The slope of the curve can be obtained by calculating the first derivative at $x = x_i$.

$$\left.\frac{\mathrm{d}y}{\mathrm{d}x}\right|_{x=x_i} = 1 \tag{4-5}$$

The description of the tangent line through the inflection point is:

$$y = x \tag{4-6}$$

(2) Double exponential function

The double exponential function is given as:

$$y = \exp[-\exp(-x)] \tag{4-7}$$

The first and second derivatives of Eq. (4-7) with respect to x are given as:

$$\frac{\mathrm{d}y}{\mathrm{d}x} = \exp[-\exp(-x)] \cdot \exp(-x) \tag{4-8}$$

$$\frac{\mathrm{d}^2y}{\mathrm{d}x^2} = \exp[-\exp(-x)] \cdot \exp(-x) \cdot [\exp(-x) - 1] \tag{4-9}$$

The second derivative is equal to zero at the inflection point $x = x_i$.

$$\left.\frac{\mathrm{d}^2y}{\mathrm{d}x^2}\right|_{x=x_i} = 0 \Longrightarrow x_i = 0 \tag{4-10}$$

The slope of the curve can be obtained by calculating the first derivative at $x = x_i$.

$$\left.\frac{dy}{dx}\right|_{x=x_i} = e^{-1} \tag{4-11}$$

The description of the tangent line through the inflection point is:

$$y = e^{-1}(x + 1) \tag{4-12}$$

According to the above information, the essential properties of the hyperbolic tangent and double exponential functions are depicted in Figure 4-1. One can readily see that the hyperbolic tangent function represents a symmetric sigmoidal curve with respect to one point (0, 0) and that the double exponential function is an asymmetric sigmoidal curve with respect to one point (0, e^{-1}). The first derivative of the hyperbolic tangent function is symmetric with respect to a vertical line $x = 0$, which exhibit a Gaussian distribution shape. The first derivative of the double exponential function is an asymmetric quasi-Gaussian distribution shape with a widened right-hand side. These mathematical characteristics are well consistent with the breakthrough curve. Thus, the hyperbolic tangent and double exponential functions can be used to establish new empirical breakthrough models.

4.2.2. Breakthrough models

According to the above analyses, the hyperbolic tangent and double exponential functions represent an asymptotic sigmoidal curve, which are in good agreement with the shape of the breakthrough curve. Consequently, one very reasonable scenario is that the two functions through the appropriate mathematical transformations can be used to describe the breakthrough curve. In this study, based on the stretching and translation transformations, the two parameters k and τ are introduced into the two functions to establish the new breakthrough models. The hyperbolic tangent and double exponential models (Form I) are expressed as:

$$\frac{c}{c_0} = \frac{1}{2}\{1 + \tanh[k(t - \tau)]\} \tag{4-13}$$

$$\frac{c}{c_0} = \exp\{-\exp[k(\tau - t)]\} \tag{4-14}$$

The physical meanings of the parameters k and τ are explained in detail (vide infra).

4.2.3. Modified breakthrough models

As mentioned above, the breakthrough curve has different degrees of curvature under different operating conditions. It is reported that this change in the curvature may be considered

simply by introducing n power law (Eris and Azizian, 2017). It can be seen from Figure 4-2 that the curve become steeper with the increase in n. In other words, the larger n value can represent more favorable adsorption. Thus, introduction of a dimensionless parameter n into Eq. (4-13) and Eq. (4-14) leads to the modified hyperbolic tangent and modified double exponential models (Form I).

$$\frac{c}{c_0} = \frac{1}{2^n}\{1 + \tanh[k(t-\tau)]\}^n \tag{4-15}$$

$$\frac{c}{c_0} = \langle \exp\{-\exp[k(\tau - t)]\}\rangle^n \tag{4-16}$$

In order to more completely describe a breakthrough curve and reflect its subtle changes, the parameters $\mu_{\max}$ and λ are also used to modify the above empirical breakthrough models. The detailed derivation processes are as follows.

(1) Hyperbolic tangent model (Form II)

According to the derivation procedure of Chapter 2, the first and second derivatives of the hyperbolic tangent model (Eq. (4-13)) with respect to t are given as:

$$\frac{\mathrm{d}y}{\mathrm{d}t} = \frac{k}{2}\{1 - \tanh^2[k(t-\tau)]\} \tag{4-17}$$

$$\frac{\mathrm{d}^2y}{\mathrm{d}t^2} = -k^2 \cdot \tanh[k(t-\tau)] \cdot \{1 - \tanh^2[k(t-\tau)]\} \tag{4-18}$$

The second derivative is equal to zero at the inflection point $t = t_i$.

$$\left.\frac{\mathrm{d}^2y}{\mathrm{d}t^2}\right|_{t=t_i} = 0 \Longrightarrow t_i = \tau \tag{4-19}$$

The maximum specific breakthrough rate can be calculated by substituting Eq. (4-19) into Eq. (4-17), which is given as:

$$\mu_{\max} = \left.\frac{\mathrm{d}y}{\mathrm{d}t}\right|_{t=t_i} = \frac{k}{2} \tag{4-20}$$

The description of the tangent line through the inflection point is:

$$y = \frac{k}{2}(t-\tau) + \frac{1}{2} \tag{4-21}$$

The lag time is given as:

$$\frac{k}{2}(\lambda - \tau) + \frac{1}{2} = 0 \Longrightarrow \lambda = \tau - \frac{1}{k} \tag{4-22}$$

The half-operating time t_{50} is given as:

$$t_{50} = \tau \tag{4-23}$$

Eq. (4-20) and Eq. (4-22) are rewritten as:

$$k = 2\mu_{\max} \tag{4-24}$$

$$\tau = \lambda + \frac{1}{2\mu_{\max}} \tag{4-25}$$

Substitution Eq. (4-24) and Eq. (4-25) into Eq. (4-13) leads to

$$\frac{c}{c_0} = \frac{1}{2}\{1 + \tanh[2\mu_{\max}(t - \lambda) - 1]\} \tag{4-26}$$

(2) Double exponential model (Form II)

The first and second derivatives of the double exponential model (Eq. (4-14)) with respect to t are given as:

$$\frac{\mathrm{d}y}{\mathrm{d}t} = k \cdot \exp[k(\tau - t)] \cdot \exp\{-\exp[k(\tau - t)]\} \tag{4-27}$$

$$\frac{\mathrm{d}^2y}{\mathrm{d}t^2} = k^2 \cdot \exp[k(\tau - t)] \cdot \exp\{-\exp[k(\tau - t)]\} \cdot \{\exp[k(\tau - t)] - 1\} \tag{4-28}$$

The second derivative is equal to zero at the inflection point $t = t_i$.

$$\left.\frac{\mathrm{d}^2y}{\mathrm{d}t^2}\right|_{t=t_i} = 0 \Longrightarrow t_i = \tau \tag{4-29}$$

The maximum specific breakthrough rate can be calculated by substituting Eq. (4-29) into Eq. (4-27), which is given as:

$$\mu_{\max} = \left.\frac{\mathrm{d}y}{\mathrm{d}t}\right|_{t=t_i} = k\mathrm{e}^{-1} \tag{4-30}$$

The description of the tangent line through the inflection point is:

$$y = k\mathrm{e}^{-1}(t - \tau) + \mathrm{e}^{-1} \tag{4-31}$$

The lag time is given as:

$$k\mathrm{e}^{-1}(\lambda - \tau) + \mathrm{e}^{-1} = 0 \Longrightarrow \lambda = \tau - \frac{1}{k} \tag{4-32}$$

The half-operating time t_{50} is given as:

$$t_{50} = \tau - \frac{1}{k}\ln(\ln 2) \tag{4-33}$$

Eq. (4-30) and Eq. (4-32) are rewritten as:

$$k = \mu_{\max} \mathrm{e} \tag{4-34}$$

$$\tau = \lambda + \frac{1}{\mu_{\max} \mathrm{e}} \tag{4-35}$$

Substitution Eq. (4-34) and Eq. (4-35) into Eq. (4-14) leads to

$$\frac{c}{c_0} = \exp\{-\exp[\mu_{\max} \mathrm{e}(\lambda - t) + 1]\} \tag{4-36}$$

(3) Modified hyperbolic tangent model (Form II)

The first and second derivatives of the modified hyperbolic tangent model (form I) Eq. (4-15) with respect to t are given as:

$$\frac{\mathrm{d}y}{\mathrm{d}t} = \frac{nk}{2^n} \cdot \{1 + \tanh[k(t-\tau)]\}^{n-1} \cdot \{1 - \tanh^2[k(t-\tau)]\} \tag{4-37}$$

$$\frac{\mathrm{d}^2 y}{\mathrm{d}t^2} = \frac{nk^2}{2^n} \cdot \{1 + \tanh[k(t-\tau)]\}^{n} \cdot \{1 - \tanh[k(t-\tau)]\} \cdot \{n - 1 - (n+1)\tanh[k(t-\tau)]\} \tag{4-38}$$

The second derivative is equal to zero at the inflection point $t = t_i$.

$$\left.\frac{\mathrm{d}^2 y}{\mathrm{d}t^2}\right|_{t=t_i} = 0 \Longrightarrow t_i = \tau + \frac{1}{k}\operatorname{arctanh}\left(\frac{n-1}{n+1}\right) \tag{4-39}$$

The maximum specific breakthrough rate can be calculated by substituting Eq. (4-39) into Eq. (4-37), which is given as:

$$\mu_{\max} = \left.\frac{\mathrm{d}y}{\mathrm{d}t}\right|_{t=t_i} = 2k\left(\frac{n}{n+1}\right)^{n+1} \tag{4-40}$$

The description of the tangent line through the inflection point is:

$$y = 2k\left(\frac{n}{n+1}\right)^{n+1}\left[t - \tau - \frac{1}{k}\operatorname{arctanh}\left(\frac{n-1}{n+1}\right)\right] + \left(\frac{n}{n+1}\right)^{n} \tag{4-41}$$

The lag time is given as:

$$2k\left(\frac{n}{n+1}\right)^{n+1}\left[\lambda - \tau - \frac{1}{k}\operatorname{arctanh}\left(\frac{n-1}{n+1}\right)\right] + \left(\frac{n}{n+1}\right)^{n} = 0 \Longrightarrow \lambda = \tau + \frac{1}{k}\operatorname{arctanh}\left(\frac{n-1}{n+1}\right) - \frac{n+1}{2nk} \tag{4-42}$$

The half-operating time t_{50} is given as:

$$t_{50} = \tau + \frac{1}{k}\operatorname{arctanh}\left[2^{\left(1-\frac{1}{n}\right)} - 1\right] \tag{4-43}$$

Eq. (4-40) and Eq. (4-42) are rewritten as:

$$k = \frac{\mu_{\max}}{2}\left(\frac{n+1}{n}\right)^{n+1} \tag{4-44}$$

$$\tau = \lambda + \frac{1}{k}\left[\frac{n+1}{2n} - \operatorname{arctanh}\left(\frac{n-1}{n+1}\right)\right] \tag{4-45}$$

Substitution Eq. (4-44) and Eq. (4-45) into Eq. (4-15) leads to

$$\frac{c}{c_0} = \frac{1}{2^n}\left\{1 + \tanh\left[\frac{\mu_{\max}}{2}\left(\frac{n+1}{n}\right)^{n+1}(t-\lambda) - \frac{n+1}{2n} + \operatorname{arctanh}\left(\frac{n-1}{n+1}\right)\right]\right\}^n \tag{4-46}$$

(4) Modified double exponential model (Form II)

The first and second derivatives of the modified double exponential model (Form I) Eq. (4-16) with respect to t are given as:

$$\frac{\mathrm{d}y}{\mathrm{d}t} = nk \cdot \exp[k(\tau - t)] \cdot \langle \exp\{-\exp[k(\tau - t)]\}\rangle^n \tag{4-47}$$

$$\frac{\mathrm{d}^2y}{\mathrm{d}t^2} = nk^2 \cdot \exp[k(\tau - t)] \cdot \langle \exp\{-\exp[k(\tau - t)]\}\rangle^n \cdot \{n\exp[k(\tau - t)] - 1\} \tag{4-48}$$

The second derivative is equal to zero at the inflection point $t = t_i$.

$$\left.\frac{\mathrm{d}^2y}{\mathrm{d}t^2}\right|_{t=t_i} = 0 \Longrightarrow t_i = \tau - \frac{1}{k}\ln\left(\frac{1}{n}\right) \tag{4-49}$$

The maximum specific breakthrough rate can be calculated by substituting Eq. (4-49) into Eq. (4-47), which is given as:

$$\mu_{\max} = \left.\frac{\mathrm{d}y}{\mathrm{d}t}\right|_{t=t_i} = k\mathrm{e}^{-1} \tag{4-50}$$

The description of the tangent line through the inflection point is:

$$y = k\mathrm{e}^{-1}\left[t - \tau + \frac{1}{k}\ln\left(\frac{1}{n}\right)\right] + \mathrm{e}^{-1} \tag{4-51}$$

The lag time is given as:

$$k\mathrm{e}^{-1}\left[\lambda - \tau + \frac{1}{k}\ln\left(\frac{1}{n}\right)\right] + \mathrm{e}^{-1} = 0 \Longrightarrow \lambda = \tau - \frac{1}{k}\left[1 + \ln\left(\frac{1}{n}\right)\right] \tag{4-52}$$

The half-operating time t_{50} is given as:

$$t_{50} = \tau - \frac{1}{k}\ln\left(\frac{1}{n}\ln 2\right) \tag{4-53}$$

Eq. (4-50) and Eq. (4-52) are rewritten as:

$$k = \mu_{\max}\mathrm{e} \tag{4-54}$$

$$\tau = \lambda + \frac{1}{\mu_{\max}\mathrm{e}}\left[1 + \ln\left(\frac{1}{n}\right)\right] \tag{4-55}$$

Substitution Eq. (4-54) and Eq. (4-55) into Eq. (4-16) leads to

$$\frac{c}{c_0} = \left\langle \exp\left\{-\exp\left[\mu_{\max} e(\lambda - t) + 1 + \ln\left(\frac{1}{n}\right)\right]\right\}\right\rangle^n \quad (4\text{-}56)$$

The hyperbolic tangent and double exponential models and corresponding modified models (Form I and Form II) are listed in Table 4-1. According to the above derivation processes, the mathematical relationships between the model parameters (k, τ and n) and the four defined parameters (μ_{max}, λ, t_i and t_{50}) are listed in Table 4-2.

4.3. Results and discussion

4.3.1. Mathematical chracteristics

The transformation processes of the hyperbolic tangent model are depicted in Figure 4-3. It is obvious that it can be obtained by vertical translation, vertical stretching, horizontal stretching and horizontal translation transformations successively. As shown in Figure 4-4, the double exponential model can be obtained through horizontal stretching and horizontal translation transformations. During the transformation processes, the horizontal stretching transformation indicates that the parameter k does not affect the location of the breakthrough curve but influence its degree of curvature. The breakthrough curves become steeper with the increase in k. In contrast, the horizontal translation transformation indicates that the parameter τ determines the location of the breakthrough curve alone. Therefore, the physical meanings of the parameters k and τ represent the rate constant and the operating time required to reach the inflection point t_i, respectively. It is worth noting that the hyperbolic tangent and double exponential models proposed in this study require no detailed data concerning the characteristics of the adsorbates, the type of the adsorbents and any operating conditions such as initial solute concentration, flow rate, bed height, particle size, pH and temperature. In other words, the parameters k and τ are more likely to be the lumped constants that are merely empirical, which are related to the physical processes and operating conditions.

Mathematically speaking, the stretching and translation transformations do not change the symmetry of the curve. Thus, the hyperbolic tangent model represents a symmetric sigmoidal curve at the inflection point, while the double exponential model is an asymmetric S-shaped curve. The asymmetric breakthrough curve is ascribed to the fact that the adsorption rate falls off more rapidly than the residual adsorption capacity of the adsorbent and that the adsorbent

consists of two or more constituents of unequal reactivity (Bohart and Adams, 1920).

The comparison of t_{50} with t_i is necessary to understand the symmetry of the breakthrough curve. According to Table 4-2, t_{50} and t_i is equal for the hyperbolic tangent model since its breakthrough curve is centrosymmetric. For the double exponential model and corresponding modified model, $t_i - t_{50}$ can be expressed as follows:

$$t_i - t_{50} = \frac{1}{k}\ln(\ln 2) < 0 \tag{4-57}$$

Eq. (4-57) indicates that the half-operating time t_{50} is always more than the inflection point t_i. The negative value of $t_i - t_{50}$ is independent of any parameter, implying the double exponential model and corresponding modified model only represent an asymmetric breakthrough curve. Moreover, the breakthrough curve almost coincides for the double exponential model and corresponding modified model when the parameter n varies slightly around $n = 1$. For the modified hyperbolic tangent model, $t_i - t_{50}$ can be expressed as:

$$t_i - t_{50} = \frac{1}{k}\left\{\operatorname{arctanh}\left(\frac{n-1}{n+1}\right) - \operatorname{arctanh}\left[2^{\left(1-\frac{1}{n}\right)} - 1\right]\right\} \tag{4-58}$$

As shown in Figure 4-5, conclusions can be drawn for the modified hyperbolic tangent model: $0 < n < 1$, $t_i > t_{50}$; $n = 1$, $t_i = t_{50}$; and $n > 1$, $t_i < t_{50}$. As a consequence, the modified hyperbolic tangent model can also represent an asymmetric breakthrough curve ($n \neq 1$). Predictably, the modified hyperbolic tangent model has better fitting performance because the adjusted parameter n makes the curve fitting more flexible.

The rate profiles for the hyperbolic tangent and double exponential models are described in Figure 4-6. It is observed that the breakthrough rate is always more than zero at any time ($dy/dt > 0$). The rate profile provided by the hyperbolic tangent model is symmetric with respect to a vertical line $t = \tau$, which exhibits a Gaussian distribution shape. By contrast, the rate profile offered by the double exponential model represents an asymmetric quasi-Gaussian distribution shape with a widened right-hand side. The curvature and location of the rate profile depend on the parameters k and τ, respectively.

4.3.2. Relationships between breakthrough models

It is worth noting that both hyperbolic tangent and double exponential models contain the exponential term. Therefore, it is extremely essential to explore the mathematical relationships

between them and the Yoon–Nelson model. According to Eq. (4-13), the hyperbolic tangent model is rewritten as:

$$\frac{c}{c_0} = \frac{1}{2}\left\{1 + \frac{\exp[k(t-\tau)] - \exp[-k(t-\tau)]}{\exp[k(t-\tau)] + \exp[-k(t-\tau)]}\right\} \tag{4-59}$$

Eq. (4-59) can simplify to

$$\frac{c}{c_0} = \frac{1}{1 + \exp[2k(\tau - t)]} \tag{4-60}$$

Let $k^* = 2k$, and then Eq. (4-60) can reduce to

$$\frac{c}{c_0} = \frac{1}{1 + \exp[k^*(\tau - t)]} \tag{4-61}$$

It is not difficult to find that Eq. (1-4) and Eq. (4-61) have identical mathematical forms. As a result, the breakthrough curves and rate profiles will be coincident and all error equations are also equal when the hyperbolic tangent and Yoon–Nelson models are employed to analyze the same set of the experimental data. Besides, according to Eq. (4-14), the double exponential model can be rewritten as:

$$\frac{c}{c_0} = \frac{1}{\exp\{\exp[k(\tau - t)]\}} \tag{4-62}$$

For small value of x, the following mathematical approximation is acceptable (Azizian, 2004).

$$\exp(x) \approx 1 + x \tag{4-63}$$

Eq. (4-62) can reduce to

$$\frac{c}{c_0} = \frac{1}{1 + \exp[k(\tau - t)]} \tag{4-64}$$

It is evident that the double exponential model can also reduce to the Yoon–Nelson model by the appropriate mathematical approximation. Explicating the mathematical relationships between hyperbolic tangent, double exponential and Yoon–Nelson models contributes to understanding the physical meanings of the model parameters and gaining insights into the dynamic behaviors in a fixed-bed adsorption system. Predictably, the double exponential model has better fitting performance than the hyperbolic tangent model since the breakthrough curve is usually asymmetric in the adsorption of water pollutants even for adsorption of individual solute in a fixed-bed adsorption system (Rojas-Mayorga et al., 2015).

4.3.3. Validation of breakthrough models

The fitting results of the hyperbolic tangent, double exponential and corresponding modified models are depicted in Figure 4-7. One can readily see that the fitting curves provided by the modified hyperbolic tangent model can better approach the experimental data and the predicted values are well consistent with the observed values. Moreover, it has larger Adj. R^2 and smaller χ^2 values (Table 4-3). Thus, the modified hyperbolic tangent model is superior to the hyperbolic tangent model. The parameter n = 4.50 indicates that the breakthrough curve is asymmetric. The maximum specific breakthrough rate μ_{max}, lag time λ, inflection point t_i and half-operating time t_{50} predicted by the modified hyperbolic tangent model are 3.94×10^{-3} min^{-1}, 30.0 min, 132.9 min and 157.2 min, respectively.

For the double exponential and modified double exponential models, the breakthrough curves are almost coincident and a plot of the predicted versus observed values is also almost coincident. As shown in Table 4-3, the residual parameters are almost equal except for the parameter τ. These results indicate that introduction of the parameter n few improves the fitting performance of the double exponential model. Compared with the hyperbolic tangent model, the double exponential model with larger Adj. R^2 and smaller χ^2 values can better describe the adsorption of nitrate adsorption on chitosan-Fe(III) composite. Therefore, the double exponential model is better than the hyperbolic tangent model.

4.4. Summary

The empirical breakthrough models developed in this study can well describe the adsorption of nitrate on chitosan-Fe(III) composite. The double exponential model has better fitting performance than the hyperbolic tangent model. The parameter n significantly improves the fitting performance of the hyperbolic tangent model and scarcely affects that of the double exponential model. The maximum specific breakthrough rate μ_{max}, lag time λ, inflection point t_i and half-operating time t_{50} can more completely describe the breakthrough curve. The hyperbolic tangent model exhibits a symmetric Gaussian distribution shape of the rate profile, while the double exponential model represents an asymmetric quasi-Gaussian distribution shape with a widened right-hand side. These empirical models represent different types of the

breakthrough curves and thus they can describe the adsorption behaviors over a large range of waster pollutants and operating conditions.

Table 4-1 Empirical breakthrough models and the corresponding modified models.

Model	Form I	Form II
Hyperbolic tangent	$\frac{c}{c_0} = \frac{1}{2}\{1 + \tanh[k(t-\tau)]\}$	$\frac{c}{c_0} = \frac{1}{2}\{1 + \tanh[2\mu_{\max}(t-\lambda) - 1]\}$
Double exponential	$\frac{c}{c_0} = \exp\{-\exp[k(\tau - t)]\}$	$\frac{c}{c_0} = \exp\{-\exp[\mu_{\max}\mathrm{e}(\lambda - t) + 1]\}$
Modified hyperbolic tangent	$\frac{c}{c_0} = \frac{1}{2^n}\{1 + \tanh[k(t-\tau)]\}^n$	$\frac{c}{c_0} = \frac{1}{2^n}\left\{1 + \tanh\left[\frac{\mu_{\max}}{2}\left(\frac{n+1}{n}\right)^{n+1}(t-\lambda) - \frac{n+1}{2n} + \operatorname{artanh}\left(\frac{n-1}{n+1}\right)\right]\right\}^n$
Modified double exponential	$\frac{c}{c_0} = \langle\exp\{-\exp[k(\tau - t)]\}\rangle^n$	$\frac{c}{c_0} = \langle\exp\left\{-\exp\left[\mu_{\max}\mathrm{e}(\lambda - t) + 1 + \ln\left(\frac{1}{n}\right)\right]\right\}\rangle^n$

Table 4-2 Mathematical relationships between model parameters (k, τ and n) and defined four parameters (μ_{max}, λ, t_i and t_{50}).

Parameters	Hyperbolic tangent	Modified hyperbolic tangent
μ_{max}	$\frac{k}{2}$	$2k\left(\frac{n}{n+1}\right)^{n+1}$
λ	$\tau-\frac{1}{k}$	$\tau+\frac{1}{k}\operatorname{arctanh}\left(\frac{n-1}{n+1}\right)-\frac{n+1}{2nk}$
t_i	τ	$\tau+\frac{1}{k}\operatorname{arctanh}\left(\frac{n-1}{n+1}\right)$
t_{50}	τ	$\tau+\frac{1}{k}\operatorname{arctanh}\left[2^{\left(1-\frac{1}{n}\right)}-1\right]$
Parameters	Double exponential	Modified double exponential
μ_{max}	$k\mathrm{e}^{-1}$	$k\mathrm{e}^{-1}$
λ	$\tau-\frac{1}{k}$	$\tau-\frac{1}{k}\left[1+\ln\left(\frac{1}{n}\right)\right]$
t_i	τ	$\tau-\frac{1}{k}\ln\left(\frac{1}{n}\right)$
t_{50}	$\tau-\frac{1}{k}\ln(\ln 2)$	$\tau-\frac{1}{k}\ln\left(\frac{1}{n}\ln 2\right)$

Table 4-3 Errors and parameters obtained from the hyperbolic tangent and double exponential models and corresponding modified models.

Parameters	Hyperbolic tangent	Modified hyperbolic tangent	Double exponential	Modified double exponential
k (min^{-1})	7.73×10^{-3}	5.94×10^{-3}	1.09×10^{-2}	1.09×10^{-2}
τ (min)	163.4	6.21	121.9	89.7
n		4.50		1.42
μ_{max} (min^{-1})	4.00×10^{-3}	3.94×10^{-3}	3.99×10^{-3}	4.00×10^{-2}
λ (min)	34.0	30.0	29.7	29.8
t_i (min)	163.4	132.9	121.9	121.9
t_{50} (min)	163.4	157.2	155.7	155.6
Adj. R^2	0.9878	0.9960	0.9977	0.9976
χ^2	1.37×10^{-3}	4.52×10^{-4}	2.54×10^{-4}	2.65×10^{-4}

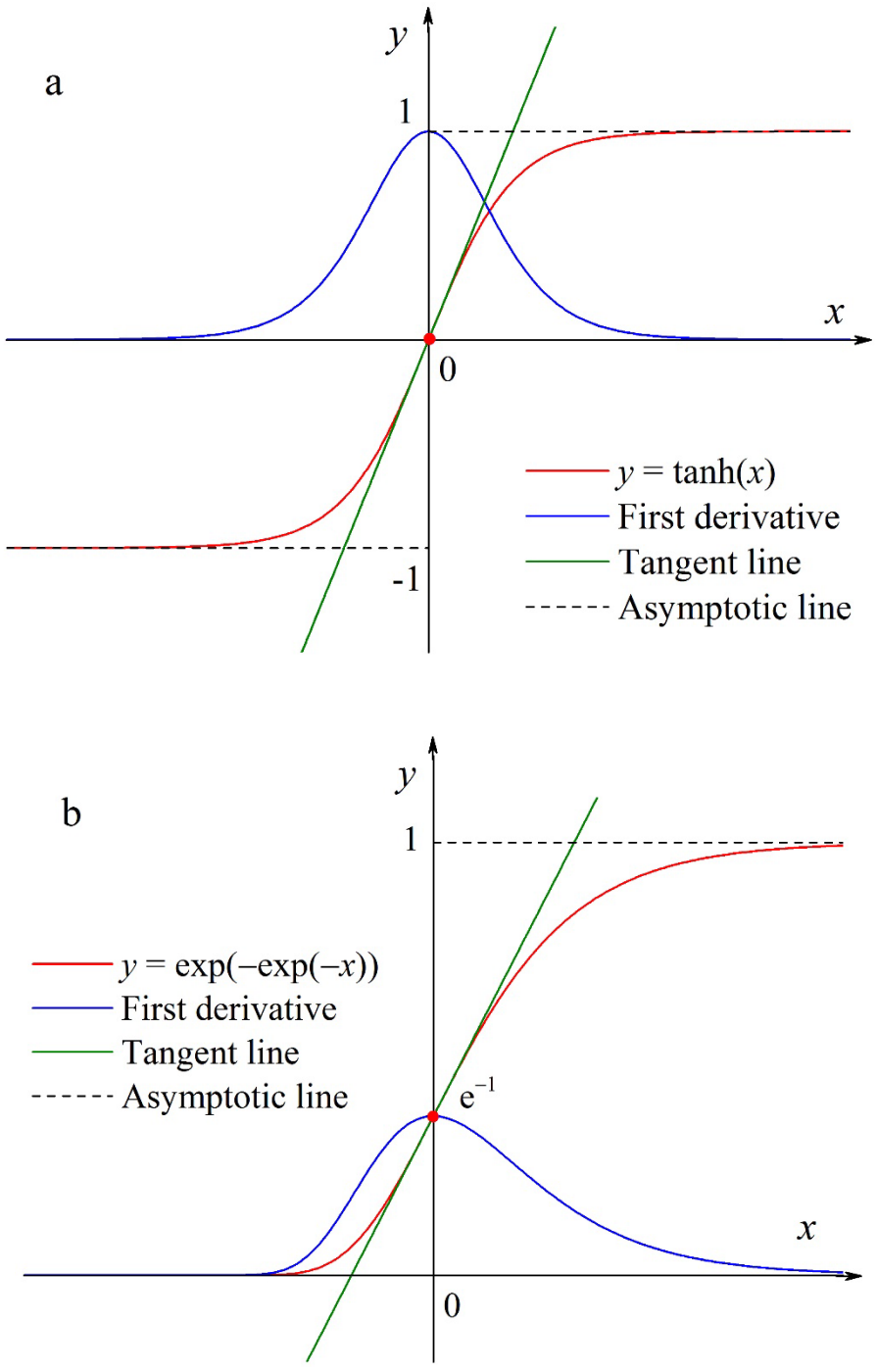

Figure 4-1 Schematic diagram of (a) hyperbolic tangent and (b) double exponential functions.

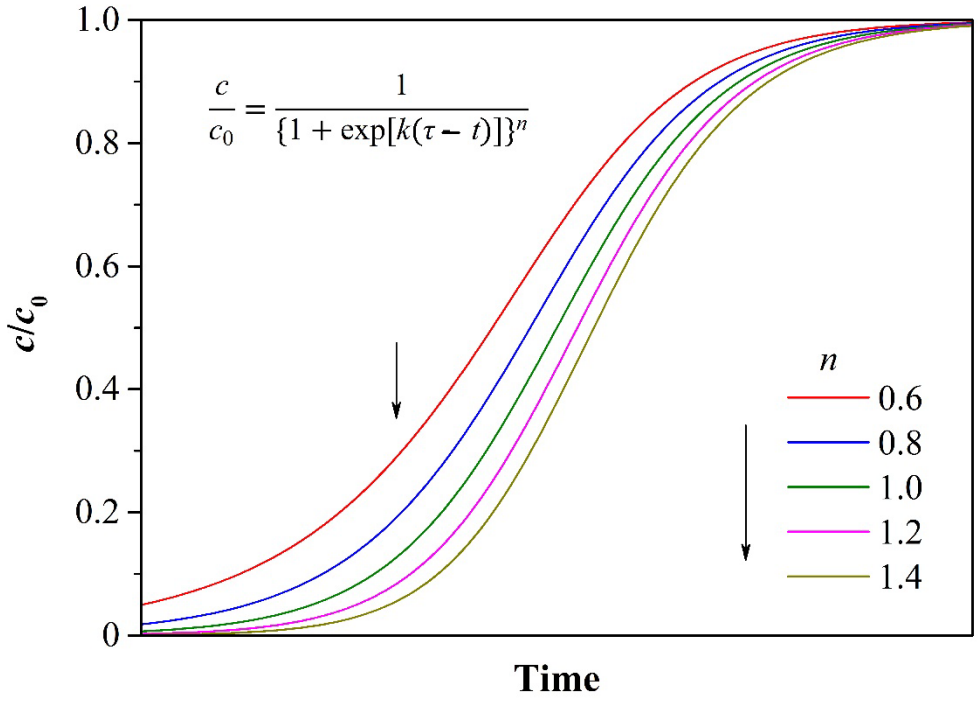

Figure 4-2 Schematic diagram for the effect of the parameter *n* on the breakthrough curve.

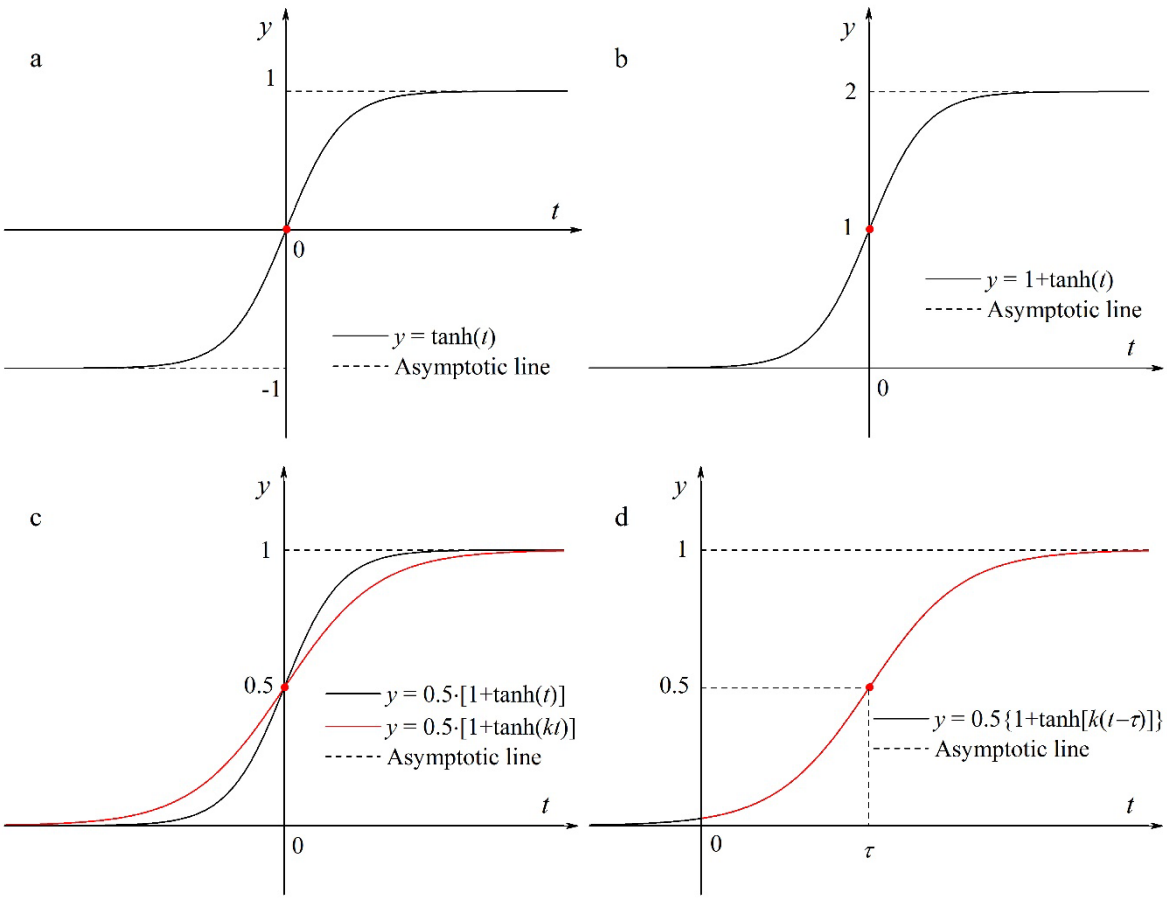

Figure 4-3 Transformation processes of the hyperbolic tangent model (a → b → c → d).

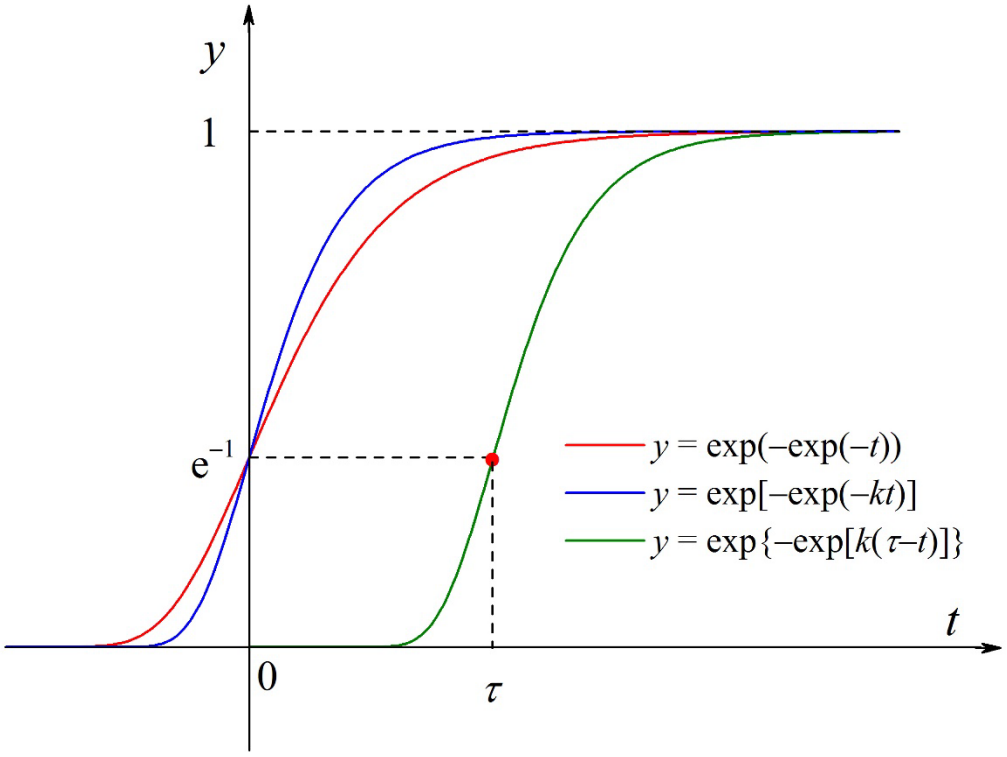

Figure 4-4 Transformation processes of the double exponential model.

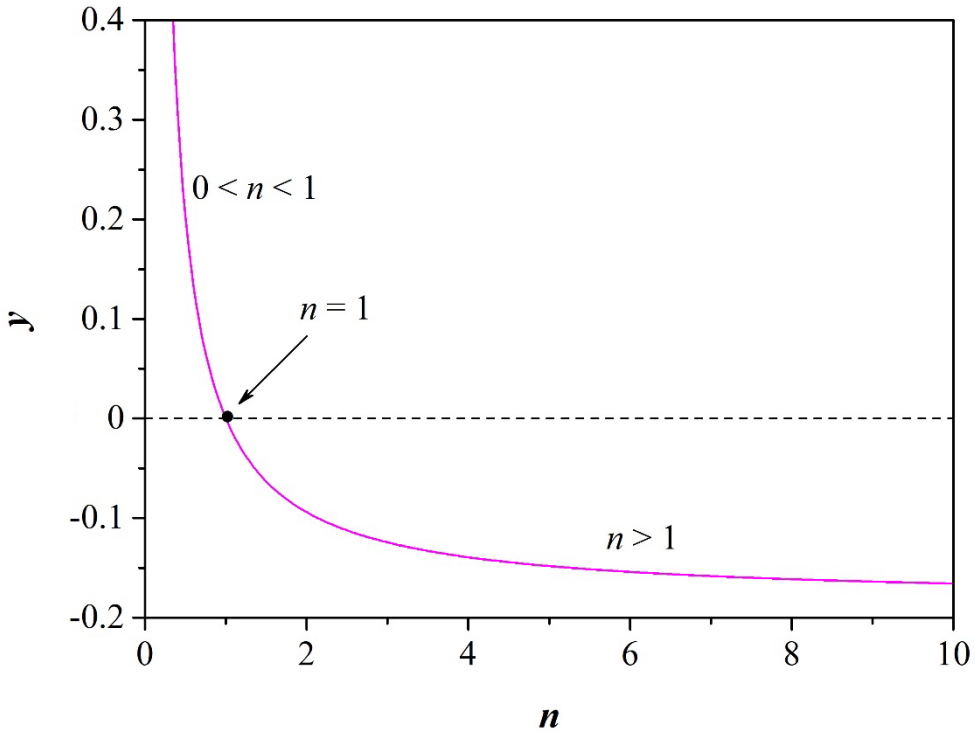

Figure 4-5 A plot of y as a function of n for the modified hyperbolic model ($y = t_i - t_{50}$).

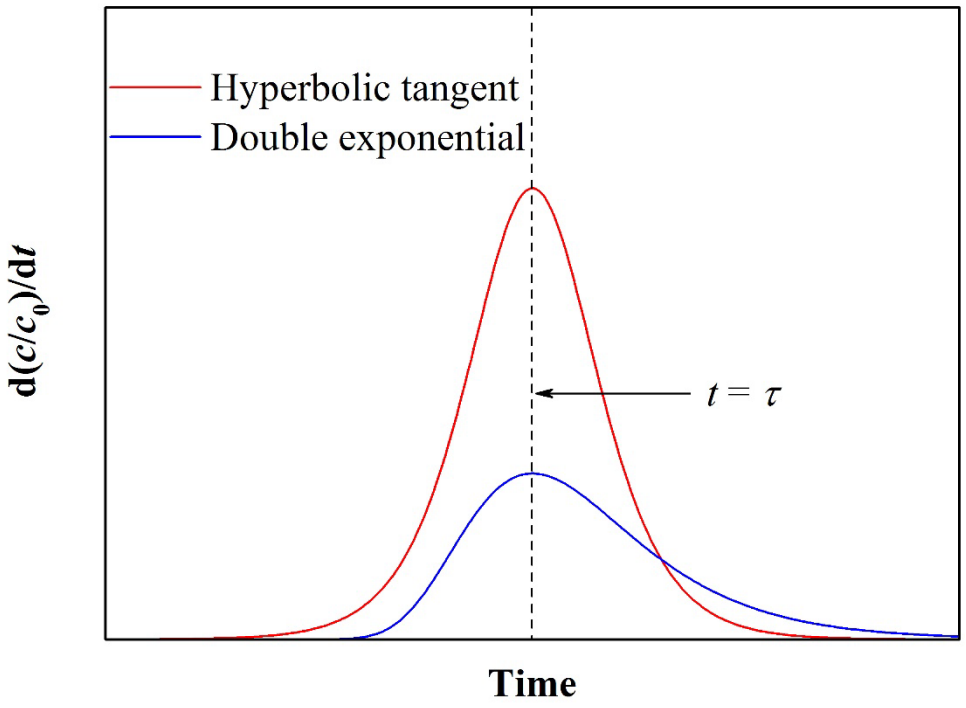

Figure 4-6 Rate profiles of hyperbolic tangent and double exponential models.

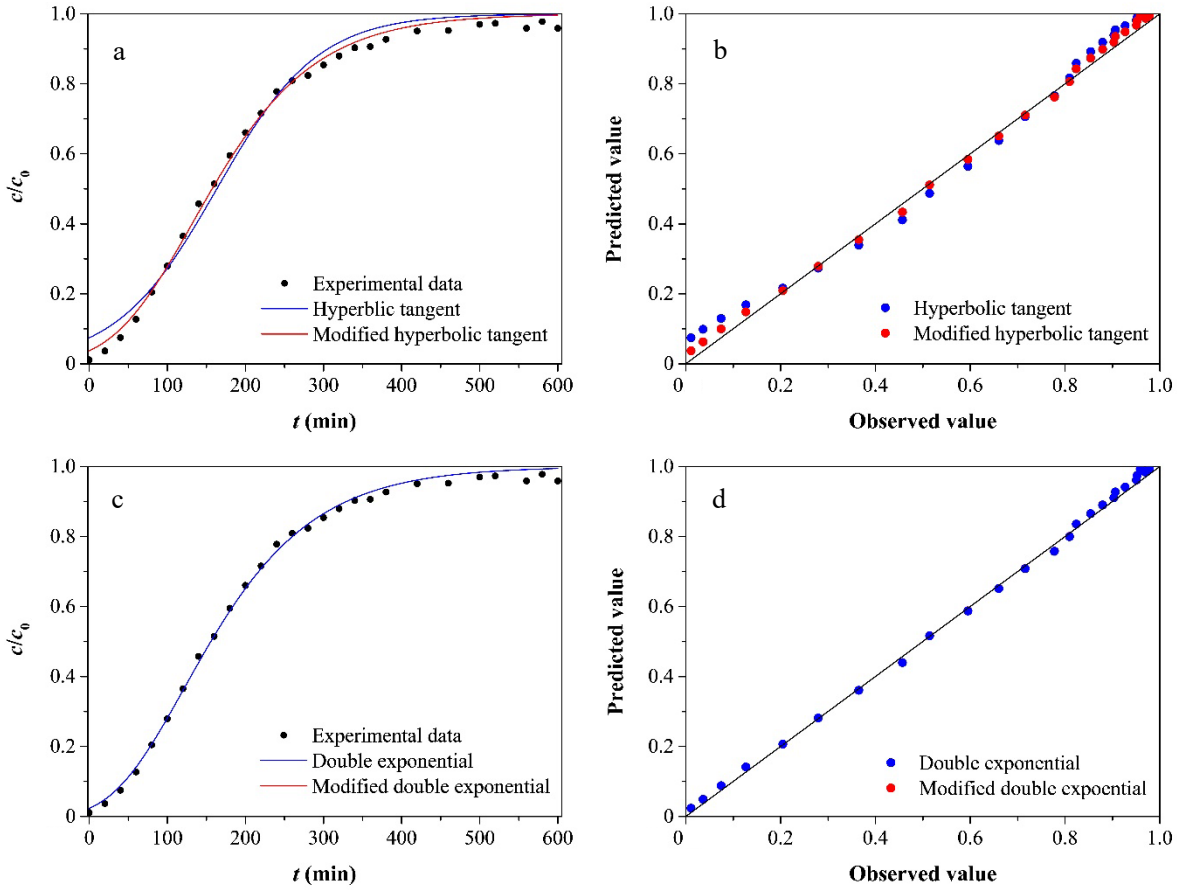

Figure 4-7 Modeling of nitrate adsorption on chitosan-Fe(III) composite using hyperbolic tangent, double exponential models and corresponding modified models: (a and c) breakthrough curve and (b and d) predicted versus observed values.

Chapter 5 Conclusions and future research

5.1. Conclusions

In this study, maximum specific breakthrough rate μ_{max}, lag time λ, inflection point t_i and half-operating time t_{50} are defined to more completely reveal mathematical characteristics of the breakthrough curve such as the degree of curvature and the symmetry. The modified Bohart–Adams, Thomas, Yoon–Nelson, Clark, and dose-response models established by substituting model parameters and operating conditions with μ_{max} and λ provide alternative methods for the modeling of fixed-bed adsorption systems. The Bohart–Adams, Thomas and Yoon–Nelson models represent a logistic function in mathematical nature and thus provide the same breakthrough curve, rate profile and error values. The Clark model can be regarded as a generalized form of the above three breakthrough models ($n = 2$) and it can provide an asymmetric breakthrough curve ($n > 1$ and $n \neq 2$). The dose-response model represents a sigmoidal curve only when the parameter a is more than unity ($a > 1$). The Wolborska model does not represent a complete sigmoidal curve and thus it is not suitable to describe the breakthrough curve within the adsorption time range. The revelation of mathematical relationships between the breakthrough models is beneficial to select the optimal model and reduce the calculated amount significantly. The graphic description of effects of model parameters on the breakthrough curves and rate profiles can more intuitively exhibit the curve characteristics. The physical meanings of the terms q_0m/vc_0 and a_0x/uc_0 are the operating time required to reach 50% breakthrough, and k_{YN} is numerically equal to a product of k_T (k_{BA}) and c_0.

In Chapter 2, the Bohart–Adams, Thomas and Yoon–Nelson models usually assume that the rate constant is independent of the operating time. However, they are not suitable to describe the heterogeneous diffusion-limited process. In order to address this problem, the introduction of the fractal-like kinetics or time-dependent rate coefficient into Bohart–Adams, Thomas and Yoon–Nelson models results in the fractal-like Bohart–Adams, fractal-like Thomas and fractal-like Yoon–Nelson models. The fractal-like Bohart–Adams and fractal-like Thomas models represent the same breakthrough curve and rate profile. Compared with the Bohart–Adams and

Yoon–Nelson models (Adj. R^2 = 0.9878 and χ^2 = 1.37 × 10^{-3}), the fractal-like Bohart–Adams (Adj. R^2 = 0.9989 and χ^2 = 1.25 × 10^{-4}) and fractal-like Yoon–Nelson (Adj. R^2 = 0.9992 and χ^2 = 8.86 × 10^{-5}) models can better describe nitrate adsorption on chitosan-Fe(III) composite. The fractal-like Bohart–Adams, fractal-like Thomas and fractal-like Yoon–Nelson models can represent an asymmetric breakthrough curve due to the introduction of the fractal-like exponent *h*, which is usually consistent with the adsorption of water pollutants. The decrease in the parameter *h* leads to the stepper breakthrough curves and rapid adsorption rate.

In Chapter 3, it is extremely necessary to establish the empirical breakthrough models based on some sigmoidal functions because the existing breakthrough models are not likely to describe all adsorbent-adsorbate systems. The empirical breakthrough models developed in this study include the hyperbolic tangent, double exponential models and corresponding modified models. The hyperbolic tangent model represents a symmetric breakthrough model and the residual three empirical models represent an asymmetric breakthrough curve. These empirical models can describe nitrate adsorption on chitosan-Fe(III) composite well except the hyperbolic tangent model. The parameter *n* significantly improves the fitting performance of the hyperbolic tangent model and scarcely affects that of the double exponential model. These empirical breakthrough models represent different types of the breakthrough curves and thus they provide an alternative method for the modeling of fixed-bed adsorption systems.

In Chapter 4, faced with different adsorbent-adsorbate systems, the degree of curvature and symmetry of the breakthrough curves tend to have significant differences. It is widely accepted that if the intraparticle diffusion is the rate-controlling step, the adsorption rate falls off more rapidly than the residual adsorption capacity of the adsorbent or the adsorbent consists of two or more constituents of unequal reactivity, the breakthrough curves are usually asymmetric. The appropriate design of an adsorption process requires the development of a mathematical model that can describe the dynamic adsorption behaviors and predict the breakthrough curve. The fractal-like and empirical breakthrough models proposed in this work may provide alternative methods for the modeling of these adsorption systems and they are important supplements of the adsorption kinetics. In particular, the fractal-like Bohart–Adams, fractal-like Thomas, fractal-like Yoon–Nelson and double exponential models can provide

asymmetric breakthrough curves, which can better describe the adsorption of a wide range of water pollutants. It should be noted that the fractal-like breakthrough models have the best fitting performance among numerous breakthrough models because the adsorption of water pollutants is often heterogeneous diffusion-limited adsorption process.

5.2. Future research

A study of breakthrough models in a continuous-flow fixed-bed column is still a hot topic in the adsorption field. However, it is a difficult task to develop a mathematical model that can accurately describe the dynamic behaviors in a fixed-bed column. This work mainly discusses mathematical characteristics of the breakthrough curves and rate profiles, proposes the fractal-like breakthrough models to describe heterogeneous diffusion-limited adsorption process and develops empirical breakthrough models to describe different adsorbent-adsorbate systems. However, there are still many problems to be addressed, including:

(1) The fractal-like and empirical breakthrough models should be applied to the adsorption of a wide range of water pollutants and further validate the applicability of these models under different operating conditions;

(2) New empirical breakthrough models are established to adapt to the complex and variable fixed-bed adsorption systems based on different types of sigmoid functions such as arc tangent and Gudermannian functions;

(3) The mathematically rigid partial differential equations are established to describe the mass and heat balance in a fixed-bed column.

References

Ahmed, M.J., Hameed, B.H. 2018. Removal of emerging pharmaceutical contaminants by adsorption in a fixed-bed column: A review. Ecotoxicology and Environmental Safety, 149, 257-266.

Alberti, G., Amendola, V., Pesavento, M., Biesuz, R. 2012. Beyond the synthesis of novel solid phases: Review on modelling of sorption phenomena. Coordination Chemistry Reviews, 256, 28-45.

Ataei-Germi, T., Nematollahzadeh, A. 2016. Bimodal porous silica microspheres decorated with polydopamine nano-particles for the adsorption of methylene blue in fixed-bed columns. Journal of Colloid and Interface Science, 470, 172-182.

Azizian, S. 2004. Kinetic models of sorption: a theoretical analysis. Journal of Colloid and Interface Science, 276, 47-52.

Bohart, G., Adams, E. 1920. Some aspects of the behavior of charcoal with respect to chlorine. Journal of the American Chemical Society, 42, 523-544.

Bonilla-Petriciolet, A., Mendoza-Castillo, D.I., Reynel-Ávila, H.E. 2017. *Adsorption Processes for Water Treatment and Purification*. Springer International Publishing, 20-24.

Carabineiro, S.A.C., Thavorn-Amornsri, T., Pereira, M.F.R., Figueiredo, J.L. 2011. Adsorption of ciprofloxacin on surface-modified carbon materials. Water Research, 45, 4583-4591.

Çeçen, F., Aktas, Ö. 2011. *Activated Carbon for Water and Wastewater Treatment: Integration of Adsorption and Biological Treatment*. Wiley-VCH Verlag GmbH and Co. KGaA, 13-42.

Chu, K.H. 2004. Improved fixed bed models for metal biosorption. Chemical Engineering Journal, 97, 233-239.

Chu, K.H. 2010. Fixed bed sorption: Setting the record straight on the Bohart–Adams and Thomas models. Journal of Hazardous Materials, 177, 1006-1012.

Clark, R.M. 1987. Evaluating the cost and performance of field-scale granular activated carbon systems. Environmental Science and Technology, 21, 573-580.

Darweesh, T.M., Ahmed, M.J. 2017. Adsorption of ciprofloxacin and norfloxacin from aqueous

solution onto granular activated carbon in fixed bed column. Ecotoxicology and Environmental Safety, 138, 139-145.

de Franco, M.A.E., de Carvalho, C.B., Bonetto, M.M., Soares, R.d.P., Féris, L.A. 2017. Removal of amoxicillin from water by adsorption onto activated carbon in batch process and fixed bed column: Kinetics, isotherms, experimental design and breakthrough curves modelling. Journal of Cleaner Production, 161, 947-956.

Eris, S., Azizian, S. 2017. Analysis of adsorption kinetics at solid/solution interface using a hyperbolic tangent model. Journal of Molecular Liquids, 231, 523-527.

Figaro, S., Avril, J.P., Brouers, F., Ouensanga, A., Gaspard, S. 2009. Adsorption studies of molasse's wastewaters on activated carbon: Modelling with a new fractal kinetic equation and evaluation of kinetic models. Journal of Hazardous Materials, 161, 649-656.

Foo, K.Y., Hameed, B.H. 2010. Insights into the modeling of adsorption isotherm systems. Chemical Engineering Journal, 156, 2-10.

Gong, J.L., Zhang, Y.L., Jiang, Y., Zeng, G.M., Cui, Z.H., Liu, K., Deng, C.H., Niu, Q.Y., Deng, J.H., Huan, S.Y. 2015. Continuous adsorption of Pb(II) and methylene blue by engineered graphite oxide coated sand in fixed-bed column. Applied Surface Science, 330, 148-157.

Haerifar, M., Azizian, S. 2014. Fractal-like kinetics for adsorption on heterogeneous solid surfaces. The Journal of Physical Chemistry C, 118, 1129-1134.

Harter, R.D. 1984. Curve-fit errors in Langmuir adsorption maxima. Soil Science Society of America Journal, 48, 749-752.

Hossein-Zadeh, N.G. 2015. Modeling the growth curve of Iranian Shall sheep using non-linear growth models. Small Ruminant Research, 130, 60-66.

Hutchins, R.A. 1973. New method simplifies design of activated carbon systems. Chemical Engineering, 80, 133-138.

Jang, J., Lee, D.S. 2016. Enhanced adsorption of cesium on PVA-alginate encapsulated Prussian blue-graphene oxide hydrogel beads in a fixed-bed column system. Bioresource Technology, 218, 294-300.

Kopelman, R. 1986. Rate processes on fractals: Theory, simulations, and experiments. Journal of Statistical Physics, 42, 185-200.

Kopelman, R. 1988. Fractal reaction kinetics. Science, 241, 1620-1626.

Kundu, S., Gupta, A.K. 2005. Analysis and modeling of fixed bed column operations on As(V) removal by adsorption onto iron oxide-coated cement (IOCC). Journal of Colloid and Interface Science, 290, 52-60.

Loganathan, P., Vigneswaran, S., Kandasamy, J. 2013. Enhanced removal of nitrate from water using surface modification of adsorbents – A review. Journal of Environmental Management, 131, 363-374.

Machado, F.M., Bergmann, C.P., Fernandes, T.H.M., Lima, E.C., Royer, B., Calvete, T., Fagan, S.B. 2011. Adsorption of Reactive Red M-2BE dye from water solutions by multi-walled carbon nanotubes and activated carbon. Journal of Hazardous Materials, 192, 1122-1131.

Montagnaro, F., Balsamo, M. 2014. Deeper insights into fractal concepts applied to liquid-phase adsorption dynamics. Fuel Processing Technology, 128, 412-416.

Nandanwar, S.U., Coldsnow, K., Porter, A., Sabharwall, P., Eric Aston, D., McIlroy, D.N., Utgikar, V. 2017. Adsorption of radioactive iodine and krypton from off-gas stream using continuous flow adsorption column. Chemical Engineering Journal, 320, 222-231.

Nguyen, T.A.H., Ngo, H.H., Guo, W.S., Pham, T.Q., Li, F.M., Nguyen, T.V., Bui, X.T. 2015. Adsorption of phosphate from aqueous solutions and sewage using zirconium loaded okara (ZLO): Fixed-bed column study. Science of The Total Environment, 523, 40-49.

Preethi, J., Prabhu, S.M., Meenakshi, S. 2017. Effective adsorption of hexavalent chromium using biopolymer assisted oxyhydroxide materials from aqueous solution. Reactive and Functional Polymers, 117, 16-24.

Ramos, S.N.d.C., Xavier, A.L.P., Teodoro, F.S., Gil, L.F., Gurgel, L.V.A. 2016. Removal of cobalt(II), copper(II), and nickel(II) ions from aqueous solutions using phthalate-functionalized sugarcane bagasse: Mono- and multicomponent adsorption in batch mode. Industrial Crops and Products, 79, 116-130.

Rojas-Mayorga, C.K., Bonilla-Petriciolet, A., Sánchez-Ruiz, F.J., Moreno-Pérez, J., Reynel-

Ávila, H.E., Aguayo-Villarreal, I.A., Mendoza-Castillo, D.I. 2015. Breakthrough curve modeling of liquid-phase adsorption of fluoride ions on aluminum-doped bone char using micro-columns: Effectiveness of data fitting approaches. Journal of Molecular Liquids, 208, 114-121.

Rouquerol, J., Rouquerol, F., Llewellyn, P., Maurin, G., Sing, K.S. 2013. *Adsorption by Powders and Porous Solids: Principles, Methodology and Applications*. Academic Press, 1-10.

Sana, D., Jalila, S. 2017. A comparative study of adsorption and regeneration with different agricultural wastes as adsorbents for the removal of methylene blue from aqueous solution. Chinese Journal of Chemical Engineering, 25, 1282-1287.

Shafeeyan, M.S., Wan Daud, W.M.A., Shamiri, A. 2014. A review of mathematical modeling of fixed-bed columns for carbon dioxide adsorption. Chemical Engineering Research and Design, 92, 961-988.

Shahbazi, A., Younesi, H., Badiei, A. 2011. Functionalized SBA-15 mesoporous silica by melamine-based dendrimer amines for adsorptive characteristics of Pb(II), Cu(II) and Cd(II) heavy metal ions in batch and fixed bed column. Chemical Engineering Journal, 168, 505-518.

Sheng, L., Zhang, Y., Tang, F., Liu, S. 2018. Mesoporous/microporous silica materials: Preparation from natural sands and highly efficient fixed-bed adsorption of methylene blue in wastewater. Microporous and Mesoporous Materials, 257, 9-18.

Sircar, S., Kumar, R. 1983. Adiabatic adsorption of bulk binary gas mixtures: Analysis by constant pattern model. Industrial and Engineering Chemistry Process Design and Development, 22, 271-280.

Soto, M.L., Moure, A., Domínguez, H., Parajó, J.C. 2017. Batch and fixed bed column studies on phenolic adsorption from wine vinasses by polymeric resins. Journal of Food Engineering, 209, 52-60.

Sun, X., Imai, T., Sekine, M., Higuchi, T., Yamamoto, K., Kanno, A., Nakazono, S. 2014. Adsorption of phosphate using calcined Mg_3–Fe layered double hydroxides in a fixed-bed column study. Journal of Industrial and Engineering Chemistry, 20, 3623-3630.

Tan, K.L., Hameed, B.H. 2017. Insight into the adsorption kinetics models for the removal of contaminants from aqueous solutions. Journal of the Taiwan Institute of Chemical Engineers, 74, 25-48.

Tran, H.N., You, S.J., Hosseini-Bandegharaei, A., Chao, H.P. 2017. Mistakes and inconsistencies regarding adsorption of contaminants from aqueous solutions: A critical review. Water Research, 120, 88-116.

Uddin, M.T., Rukanuzzaman, M., Khan, M.M.R., Islam, M.A. 2009. Adsorption of methylene blue from aqueous solution by jackfruit (Artocarpus heteropyllus) leaf powder: A fixed-bed column study. Journal of Environmental Management, 90, 3443-3450.

Unuabonah, E.I., Olu-Owolabi, B.I., Fasuyi, E.I., Adebowale, K.O. 2010. Modeling of fixed-bed column studies for the adsorption of cadmium onto novel polymer–clay composite adsorbent. Journal of Hazardous Materials, 179, 415-423.

Wang, W., Li, M., Zeng, Q. 2015. Adsorption of chromium(VI) by strong alkaline anion exchange fiber in a fixed-bed column: Experiments and models fitting and evaluating. Separation and Purification Technology, 149, 16-23.

Weber Jr, W.J. 1984. Evolution of a technology. Journal of Environmental Engineering, 110, 899-917.

Weber Jr, W.J., Smith, E.H. 1987. Simulation and design models for adsorption processes. Environmental Science and Technology, 21, 1040-1050.

Witek-Krowiak, A., Chojnacka, K., Podstawczyk, D. 2013. Enrichment of soybean meal with microelements during the process of biosorption in a fixed-bed column. Journal of Agricultural and Food Chemistry, 61, 8436-8443.

Wolborska, A. 1989. Adsorption on activated carbon of *p*-nitrophenol from aqueous solution. Water Research, 23, 85-91.

Worch, E. 2012. *Adsorption Technology in Water Treatment: Fundamentals, Processes, and Modeling*. Walter de Gruyter, 1-176.

Yan, G., Viraraghavan, T., Chen, M. 2001. A new model for heavy metal removal in a biosorption column. Adsorption Science and Technology, 19, 25-43.

Yan, Y., An, Q., Xiao, Z., Zheng, W., Zhai, S. 2017. Flexible core-shell/bead-like alginate@PEI

with exceptional adsorption capacity, recycling performance toward batch and column sorption of Cr(VI). Chemical Engineering Journal, 313, 475-486.

Yang, Q., Zhong, Y., Li, X., Li, X., Luo, K., Wu, X., Chen, H., Liu, Y., Zeng, G. 2015. Adsorption-coupled reduction of bromate by Fe(II)–Al(III) layered double hydroxide in fixed-bed column: Experimental and breakthrough curves analysis. Journal of Industrial and Engineering Chemistry, 28, 54-59.

Yanyan, L., Kurniawan, T.A., Zhu, M., Ouyang, T., Avtar, R., Dzarfan Othman, M.H., Mohammad, B.T., Albadarin, A.B. 2018. Removal of acetaminophen from synthetic wastewater in a fixed-bed column adsorption using low-cost coconut shell waste pretreated with NaOH, HNO_3, ozone, and/or chitosan. Journal of Environmental Management, 226, 365-376.

Yoon, Y.H., Nelson, J.H. 1984. Application of gas adsorption kinetics I. A theoretical model for respirator cartridge service life. American Industrial Hygiene Association Journal, 45, 509-516.

Zwietering, M., Jongenburger, I., Rombouts, F., Van't Riet, K. 1990. Modeling of the bacterial growth curve. Applied and Environmental Microbiology, 56, 1875-1881.

Acknowledgements

I would like to sincerely express my appreciation to Prof. Zhenya Zhang for giving me an opportunity to pursue my doctoral research. I have benefited a lot from your erudition, kindness, patience, work attitude, dedication and meticulous instruction. Also, I would like to express my gratitude to Associate Prof. Zhongfang Lei and Associate Prof. Kazuya Shimizu for giving me a lot of help.

I would like to thank thesis committee members: Associate Prof. Motoo Utsumi, Associate Prof. Kazuya Shimizu, Associate Prof. Zhongfang Lei and Prof. Zhenya Zhang for your careful correction and many valuable suggestions.

Special thanks to Prof. Chuanping Feng (China University of Geosciences (Beijing)) and Prof. Yanhua Xie (Chengdu University of Technology, China).

I would like to express my gratitude for giving me a lot of help, such as Dr. Liting Hao, Dr. Ye Liu, Dr. Nan Zhang, Ms. Qian Wang, Ms. Chunzi Feng, Dr. Di Wang, Dr. Ying Wang, Dr. Tian Yuan, Dr. Xi Yuan, Dr. Xi Yang, Dr. Shuang Sun, Ms. Hui He, Ms. Jiamin Zhao, Ms. Tingting Hou, Ms. Qun Wang, Ms. Danni Yang, Dr. Yang Yu, Dr. Qiuming Pei, Mr. Boaiqi Zhang, Mr. Yuntai Zhao, Mr. Chen Shi, Mr. Yujie Fan, Mr. Zitao Guo, Mr. Xiaoshuai Li, Mr. Chenzhu Yin, Dr. Yanfei Chen.

Thanks to the staff and good learning atmosphere in University of Tsukuba. Three years of study abroad left my wonderful memories. This experience also fulfils my childhood dream. Moreover, I would like to thank the support of the China Scholarship Council.

Finally, I would like to sincerely express my appreciation to my father, my mother and my twins brother, and kinsfolk and friends who give care and help in my life.

Achievements

[1] **Hu Qili**, Zhang Zhenya, Application of Dubinin–Radushkevich isotherm model at the solid/solution interface: A theoretical analysis, Journal of Molecular Liquids, 2019, 277: 646–648 (IF = 4.561).

[2] **Hu Qili**, Xie Yanhua, Feng Chuanping, Zhang Zhenya, Prediction of breakthrough behaviors using logistic, hyperbolic tangent and double exponential models in the fixed-bed column, Separation and Purification Technology, 2019, 212: 572–579 (IF = 5.107).

[3] **Hu Qili**, Xie Yanhua, Feng Chuanping, Zhang Zhenya, Fractal-like kinetics of adsorption on heterogeneous surfaces in the fixed-bed column, Chemical Engineering Journal, 2018, 358: 1471–1478 (IF = 8.355).

[4] **Hu Qili**, Liu Ye, Feng Chuanping, Zhang Zhenya, Lei Zhongfang, Shimizu Kazuya, Predicting equilibrium time by adsorption kinetic equations and modifying Langmuir isotherm by fractal-like approach, Journal of Molecular Liquids, 2018, 268: 728–733 (IF = 4.561).

[5] **Hu Qili**, Wang Qian, Feng Chuanping, Zhang Zhenya, Lei Zhongfang, Shimizu Kazuya, Insights into mathematical characteristics of adsorption models and physical meaning of corresponding parameters, Journal of Molecular Liquids, 2018, 254: 20–25 (IF = 4.561).